

Optical Spectroscopic Observations of Gamma-Ray Blazar Candidates. VII.

Follow-up Campaign in the Southern Hemisphere

Peña-Herazo, H. A.^{1,2,3}, Marchesini, E. J.^{1,2,4,5,6}, Álvarez Crespo, N.^{1,2}, Ricci, F.⁷, Massaro, F.^{1,2}, Chavushyan, V.³, Landoni, M.⁸, Strader, J.⁹, Chomiuk, L.⁹, Cheung, C. C.¹⁰, Masetti, N.^{6,11}, Jiménez-Bailón, E.¹², D'Abrusco, R.¹⁴, Paggi, A.¹³, Milisavljevic, D.¹³, La Franca, F.⁷, Smith, H. A.¹³, Tosti, G.¹⁵

Abstract Searching for low energy counterparts of γ -rays sources is one of the major challenges in modern γ -ray astronomy. In the third Fermi source catalog about 30 % of detected sources are unidentified/unassociated Gamma-ray Sources (UGSs). We recently started an optical spectro-

scopic follow up campaign to confirm the blazar-like nature of candidates counterparts of UGSs. Here we report the spectra of **61** targets collected with the Southern Astrophysical Research Telescope (SOAR) between 2014 and the 2017. Our sample includes **33** potential counterparts of UGSs, selected on the basis of WISE colors, and **27** blazar candidates of uncertain type associated with gamma-ray sources of the last release of the Fermi catalog. We confirm the BZB nature of **20** sources lying within the positional uncertainty region of the UGSs. All the observed BCUs show blazar-like spectra, classified as 2 BZQs and **25** BZBs, for which we obtained 6 redshift estimates. Within the BCUs observations we report the redshift estimate for the BZB associated with, 3FGL J1106.4-3643 that is the second most distant BL Lac known to date, at $z \geq 1.084$.

Peña-Herazo, H. A., Marchesini, E. J., Álvarez Crespo, N., Ricci, F., Massaro, F., Chavushyan, V., Landoni, M., Strader, J., Chomiuk, L., Cheung, C. C., Masetti, N., Jiménez-Bailón, E., D'Abrusco, R., Paggi, A., Milisavljevic, D., La Franca, F., Smith, H. A., Tosti, G.

¹Dipartimento di Fisica, Università degli Studi di Torino, via Pietro Giuria 1, I-10125 Torino, Italy

²Istituto Nazionale di Fisica Nucleare, Sezione di Torino, I-10125 Torino, Italy

³Instituto Nacional de Astrofísica, Óptica y Electrónica, Apartado Postal 51-216, 72840 Puebla, México

⁴Facultad de Ciencias Astronómicas y Geofísicas, Universidad Nacional de La Plata, Paseo del Bosque, B1900FWA, La Plata, Argentina

⁵Instituto de Astrofísica de La Plata, CONICET-UNLP, CCT La Plata, Paseo del Bosque S/N, B1900FWA, La Plata, Argentina

⁶INAF - Istituto di Astrofisica Spaziale e Fisica Cosmica di Bologna, via Gobetti 101, 40129, Bologna, Italy

⁷Dipartimento di Matematica e Fisica, Università Roma Tre, via della Vasca Navale 84, I-00146, Roma, Italy

⁸INAF-Osservatorio Astronomico di Brera, Via Emilio Bianchi 46, I-23807 Merate, Italy

⁹Center for Data Intensive and Time Domain Astronomy, Department of Physics and Astronomy, Michigan State University, East Lansing, MI 48824, USA

¹⁰Space Science Division, Naval Research Laboratory, Washington, DC 20375-5352, USA

¹¹Departamento de Ciencias Físicas, Universidad Andrés Bello, Fernández Concha 700, Las Condes, Santiago, Chile

¹²Instituto de Astronomía, Universidad Nacional Autónoma de México, Apdo. Postal 877, Ensenada, 22800 Baja California, México

¹³Harvard - Smithsonian Center for Astrophysics, 60 Garden Street, Cambridge, MA 02138, USA

¹⁴Department of Physical Sciences, University of Napoli Federico II, via Cinthia 9, 80126 Napoli, Italy

¹⁵Dipartimento di Fisica, Università degli Studi di Perugia, I-06123 Perugia, Italy

Keywords galaxies: active - galaxies: BL Lacertae objects - quasars: general

1 Introduction

Since the first release of the source catalog based on observations of the Energetic Gamma Ray Experiment Telescope (EGRET) (Fichtel et al. 1999), the nature of unidentified/unassociated gamma-ray sources (UGS) was under debate. With greater effective area and better angular resolution than previous γ -ray satellites, the Large Area Telescope (LAT), onboard of the Fermi Gamma-ray Space Telescope (Atwood et al. 2009), increased the number of detected sources by an order of magnitude, revolutionizing our understanding of the gamma-ray sky in the energy range of tens of MeV to hundreds of GeV, and significantly improving the association of γ -ray sources with their low energy counterparts (see e.g. Massaro et al. 2016 for a recent review).

However, in the first *Fermi*-LAT source catalog (1FGL) about 40% of sources were still unassociated (Abdo et al. 2010a). Then the UGS population in the *Fermi*-LAT second source catalog (2FGL) decreased to about 30% (Nolan et al. 2012) and remained almost constant in the *Fermi*-LAT third source catalog (3FGL) (Acero et al. 2015). Even if the number of UGSs is still decreasing there is still a significant fraction of them that could hide new potential discoveries (Massaro et al. 2017).

Blazars show high flux and spectral variability from optical to γ -rays (in time scales from week to minutes) coupled with superluminal motions and high bolometric luminosities (up to $10^{46} - 10^{47}$ erg s $^{-1}$) and with an emission dominated by non-thermal process over the entire electromagnetic spectrum (Urry & Padovani 1995). The spectral energy distribution of blazars mainly shows two bumps, the first one peaking at low frequencies between the infrared and the ultraviolet range and the second one dominating in the γ -rays (Abdo et al. 2010b; Fossati et al. 1998; Giommi et al. 1995). The well entertained unification scenario of active galaxies explains the observed characteristics of blazars as AGN with relativistic jets pointing at a small angle with respect to our line of sight (Blandford & Rees 1978; Urry & Padovani 1995).

Blazars are distinguished on the basis of their optical spectra in two classes: BL Lacs, objects having emission lines with rest frame equivalent width $EW \leq 5 \text{ \AA}$ (Stickel et al. 1991), and Flat Spectrum Radio Quasars (FSRQs), showing optical features as in normal quasar spectra. Here we follow the Roma-BZCAT nomenclature, where BL Lac objects are label as BZB and FSRQs are labelled as BZQ (Massaro et al. 2009; Massaro et al. 2015b). It is worth mentioning that emission and/or absorption lines in BL Lacs spectra could be hidden due to their flux variations in the optical continuum in blazars, making their redshift estimate challenging (Massaro et al. 2015a).

It is worth highlighting that blazars are the dominant class of sources in the γ -ray extragalactic sky, being about 85% of the associated sources in 3FGL (Acero et al. 2015), therefore we expect a significant fraction of UGSs at high Galactic latitudes ($|b| > 30^\circ$) to be blazars. Thus, in recent years, several methods and follow up observations were developed and used to search for blazar-like sources that, lying within the positional uncertainty region of UGSs, could be their low-energy counterparts (Cowperthwaite et al. 2013; Maselli et al. 2015; Massaro et al. 2015a).

Several methods were developed to find blazar-like potential counterparts of UGSs. For example, at radio frequencies, searching for compact radio sources (Petrov

et al. 2013; Schinzel et al. 2015) or objects with flat radio spectra (16) or even at low radio frequencies (i.e., below 1 GHz (Massaro et al. 2013a; Nori et al. 2014; Giroletti et al. 2016)), or using follow up observations at high frequencies in X-rays (Paggi et al. 2013; Takeuchi et al. 2013; Acero et al. 2013). In addition, at IR frequencies, using WISE colors Massaro et al. (2012c) developed a method to identify γ -ray blazar candidates that could find potential counterparts of UGSs thanks to an infrared γ -ray connection (Massaro & D’Abrusco 2016; Massaro et al. 2011). Several catalogs of UGSs potential counterparts were built on the basis of this IR analysis (Massaro et al. 2012a).

However none of these methods offer a conclusive way to clarify the nature of the selected potential counterparts, unless there is an optical spectroscopic confirmation. Thus, in 2013 we started an optical follow up campaign to obtain the spectra of selected blazar like counterparts for UGSs. In addition to the UGSs, we also observed Blazar Candidates of Uncertain Type (BCUs), as defined and associated in the *Fermi* catalogs i.e. *Fermi* sources with an assigned counterpart showing a multifrequency behavior similar to blazars but lacking a spectroscopic classification (Acero et al. 2015; Ackermann et al. 2015). The BCU definition in the 3FGL and in the third LAT catalog of AGNs (3LAT) corresponds to the old class of Active Galaxies of Uncertain type (AGUs) listed in the previous 1FGL and 2FGL *Fermi* catalogs (Álvarez Crespo et al. 2016c). To date we identified 223 blazars of which 173 are BZBs, additionally we have measured 49 redshifts and found 2 BZBs with $z > 1$, see Massaro et al. (2016) for a recent review.

In this paper we present the last results of the spectroscopic observations of our campaign, focused in the southern hemisphere and acquired with the Southern Astrophysical Research Telescope (SOAR) between 2014–2017. The paper is organised as follows. In section 2 we present the sample description, while in section 3 we describe the observations and the data reduction procedure. Results of our spectroscopic observations are presented in section 4. Finally section 5 is devoted to the summary and conclusions.

Throughout this work we used cgs units unless stated otherwise and we regard as flat spectrum those sources with spectral index $\alpha < 0.5$, where α is defined as the flux density $S_\nu \propto \nu^{-\alpha}$.

2 Sample Description

The main aim of our campaign is to clarify the nature of blazar-like sources lying within the positional uncertainty region of UGSs and BCUs listed in the latest release of the *Fermi* catalog via optical spectroscopic observations. Sources observed during our follow up campaign

were selected from the catalogs of WISE potential counterparts (D’Abrusco et al. 2013; D’Abrusco et al. 2014) on the basis of their visibility during the available nights and with an airmass lower than 1.5 (Massaro et al. 2015c; Landoni et al. 2015).

The sample presented in the current work consists of **61** sources grouped in three categories: UGSs, BCUs and known blazars, as described below.

1. **Thirty-three** of our sources are blazar-like potential counterparts of UGSs selected with the WISE colors, all of them are listed in the 3FGL catalog with the exception of 1FGL J1129.2-0528.
2. Nearly half of our sample (**27** out of 61) are BCUs, with counterparts in the X-rays and/or flat radio spectrum, all of them are included in the 3FGL catalog except the source 2FGL J1922.6-7454.
3. We pointed an additional source, the BZCAT object **5BZB J0814-1012** (3FGL J0814.1-1012), which is associated with the radio source NVSS J081411-101208 in 3FGL. This source already observed and classified by Álvarez Crespo et al. (2016b) was pointed because being a BL Lac we tried to get a redshift estimate hoping to observe it during a low flux state.

It is worth mentioning that 37 of our selected targets have Galactic latitude $|b| < 30^\circ$, and 7 of them have $|b| < 10^\circ$. All the sources are listed in Table 1, including its Fermi name, counterpart name and the observational log. For those we were able to estimate its redshift we reported it and for those we were not able we marked them with a quotation mark. Additionally we report its classification and finally show multifrequency notes for each objects to point up in their broad band detections.

3 Observations and Data Reduction

The strategy for our follow up campaign consists in observing small samples of potential counterparts each observing run to minimize the impact on telescope schedules. A detailed explanation of the observing strategy used during the campaign is presented in Massaro et al. (2016).

All the spectra reported in this work were acquired at the Southern Astrophysical Research Telescope (SOAR) 4.1 m telescope, at Cerro Pachón, Chile. We performed both visitor and remote mode observations. We used the Goodman High Throughput spectrograph (Clemens et al. 2004) to acquire the spectra in single slit mode, with a slit width of $1''$ and the 400 l mm^{-1} grating, obtaining a dispersion of $\sim 2 \text{ \AA pixel}^{-1}$. The observations were taken in a time span between

December 2014 up to January 2017 as shown in the Table 1.

For each source we acquired at least two exposures, and reduced them using standard IRAF standards reduction techniques (Tody 1986). We performed the bias and flat fielding corrections, and cosmic rays removal. In addition, we acquired calibration spectra of a Hg-Ar or Fe-Ar lamp for each source to calibrate the dispersion, achieving an accuracy of $0.1 - 0.5 \text{ \AA rms}$. During each night we observed at least one spectrophotometric star to perform relative flux calibration. Furthermore, we corrected the spectra by galactic extinction using the reddening law of Cardelli et al. (1989) and values of E_{B-V} computed by Schlegel et al. (1998). Finally, to highlight the spectroscopic features for visual inspection we normalised the spectra to the local continuum. In the Figures 1- 61 we report the spectra and the correspondent finding charts, while both the log and the results of our observations are reported in Table 1. In addition, we report the results of our spectroscopic observations in Table 1.

4 Results

All sources are listed in 3FGL with the only exceptions of UGS 1FGL J1129.2-0528 and the BCU 2FGL J1922.6-7454. We present below our results divided in the three categories of our sample.

4.1 Unidentified Gamma-ray Sources

Out of **33** UGSs in our sample, **20** of them show a BZB spectrum. We were not able to estimate the redshift for all of them with a single exception, WISE J012152.69-391544.2 which is the potential counterpart of 3FGL J0121.8-3917, with Ca II H & K lines visible at $\lambda_{obs} = 5438 - 5518 \text{ \AA}$ and $EW_{obs} = 1.5 - 1.02 \text{ \AA}$ leading to a redshift of $z = 0.390$ (see Table 1). The remaining **19** objects shows featureless blue spectra typical of a BZB.

Within the UGSs sample 7 blazar-like candidates have a quasar spectra but none of them has a radio counterpart in NVSS, SUMSS, FIRST (Condon et al. 1998; Mauch et al. 2003; Becker et al. 1995; White et al. 1997) and in the radio follow up performed by Petrov et al. (2013) and Schinzel et al.(2015). The lack of radio detections does not allow us to classify them as BZQs. We also found 6 objects with galaxy-like spectrum. QSOs and the galaxies could be considered contaminants of the selection procedures of UGSs counterparts (D’Abrusco et al. 2013; Massaro et al. 2013a; Massaro et al. 2013b). We list all the UGS in Table 1 along with their classification and redshift estimates.

4.2 Blazar Candidates of Uncertain Type

In our sample there are 27 BCUs and for all of them we confirm a blazar nature thanks to our follow up spectroscopic observations. Within the sample we found two candidates with QSO spectra. The first one is the candidate WISE J080311.45-033554.5, counterpart of 3FGL J0803.3-0339, showing [OII] λ 3727 emission line with $EW_{obs} = 17 \text{ \AA}$ enabling us to estimate its redshift at $z=0.365$, while the second one is WISE J161717.91-584808.0 counterpart of 3FGL J1617.4-5846 that shows broad MgII λ 2798 and the blending of SiIII λ 1892 with CIII λ 1909, respectively, giving a $z = 1.423$.

The remaining 25 BCUs show a BZB spectra and for 6 of them it was also possible to estimate their redshifts or a lower limit of their redshift given the detection of interstellar absorption features usually seen in BL Lac spectra (Sbarufatti et al. 2006). In detail, for WISE J064933.60-313920.3 counterpart of 3FGL J0649.6-3138, and associated with the X-ray source 1RXS J064933.8-313914 for which we estimated a lower limit for its redshift of $z \geq 0.563$ using the Ca II H&K absorption lines. Meanwhile for the target J100850.54-313905.5 counterpart of 3FGL J1009.0-3137 we estimate its redshift at $z = 0.534$ based on the [OII] λ 3727 emission line ($EW_{obs} = 1.4 \text{ \AA}$) and Ca II H&K absorption doublet at ($EW_{obs} = 0.7 - 0.4 \text{ \AA}$).

The third BCU is WISE J120317.88-392620.9, counterpart of 3FGL J1203.5-3925, for which we estimated a redshift of 0.227, based on the [OII] λ 3727 emission ($EW_{obs} = 3.2 \text{ \AA}$), Ca II H&K absorption lines ($EW_{obs} = 3.3 - 2.0 \text{ \AA}$) and the [OIII] doublet emission line ($EW_{obs} = 2.0 - 4.2 \text{ \AA}$). The fourth BCU is the associated to 3FGL J1312.7-2349, WISE J131248.76-235047.3, we estimated the lower limit of its redshift at $z \geq 0.462$ showing the Mg II absorption lines ($EW_{obs} = 3.2 - 2.9 \text{ \AA}$) and the doublet of Ca II H&K absorption lines ($EW_{obs} = 0.6 - 0.7 \text{ \AA}$). Finally, for the BCU, WISE J195500.65-160338.4, counterpart of 3FGL J1955.0-1605, we estimated a lower limit for its redshift at $z \geq 0.630$ using the doublet of Mg II ($EW_{obs} = 2.0 - 1.6 \text{ \AA}$).

We found that WISE J110624.04-364658.9 associated with 3FGL J1106.4-3643 in the 3FGL/3LAC, is a high redshift BZB at $z \geq 1.084$, estimated from the multiplet of Fe II absorption lines and the Mg II doublet absorption lines ($EW_{obs} = 6.2 - 5.4 \text{ \AA}$). This is the second most distant BZB to date (Massaro et al. 2016).

4.3 Other targets

Finally, we report the observation of 3FGL J0814.1-1012 associated with the radio source NVSS J081411-101208

(a.k.a. WISE J081411.69-101210.2). We confirm its nature/classification as BZB but its spectrum does not have any spectroscopic feature that allows to estimate its redshift as occurred in previous observations (Álvarez Crespo et al. 2016b).

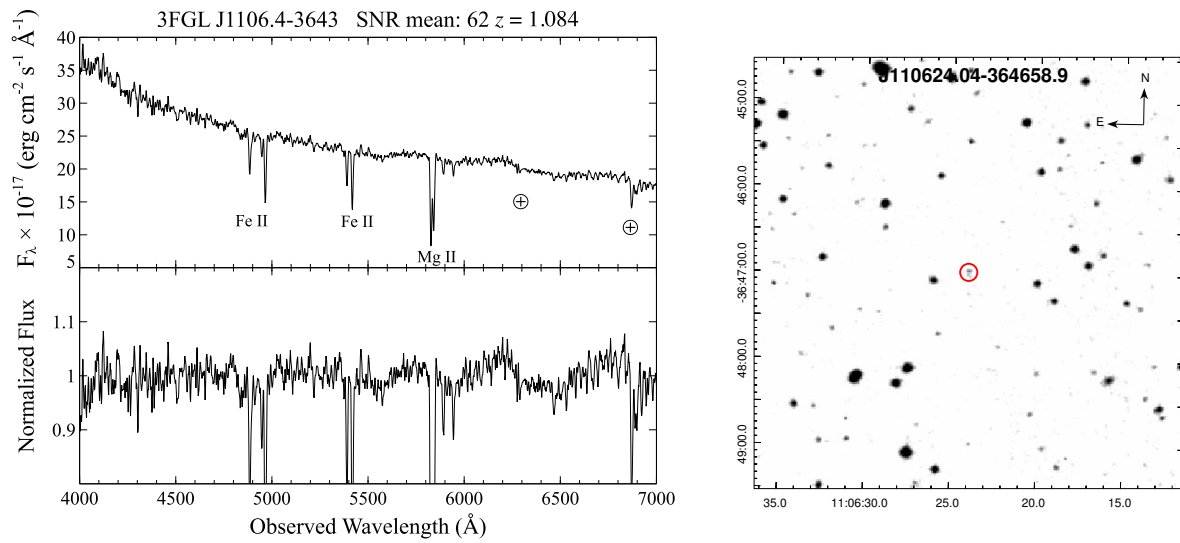


Fig. 1 (Left panel) Optical spectrum of WISE J110624.04-364658.9 associated with 3FGL J1106.4-3643, in the upper part it is shown the Signal-to-Noise Ratio of the spectrum. (Right panel) The finding chart (5' × 5') retrieved from the Digital Sky Survey highlighting the location of the counterpart: WISE J110624.04-364658.9 (red circle).

Table 1 : Observing Log and Summary of Results

Fermi Name	WISE Counterpart	R.A. (J2000) hh:mm:ss	Dec. (J2000) dd:mm:ss	Obs. Date yy-mm-dd	Exp. Time (s)	S/N	z	Class	Notes
3FGL J0121.8-3917	J012152.69-391544.2	01:21:52.70	-39:15:44.21	2016-08-02	900	41	0.390 ± 0.001	bzb	N,w,g
3FGL J0156.5-2423	J015624.54-242003.7	01:56:24.55	-24:20:03.77	2015-08-23	600	52	?	bzb	c,w,x
3FGL J0200.3-4108	J020020.94-410935.7	02:00:20.95	-41:09:35.70	2015-08-26	600	38	?	bzb	w,x
3FGL J0312.7-2222	J031235.70-222117.2	03:12:35.71	-22:21:17.21	2017-01-31	1200	71	?	bzb	N,w
3FGL J0340.4-2423	J034050.11-2422254.6	03:40:50.11	-24:22:54.66	2015-08-23	600	41	0.683 ± 0.002	qso	w
3FGL J0351.0-2816	J035051.32-281632.8	03:50:51.33	-28:16:32.81	2016-08-29	1800	45	?	bzb	N,w
3FGL J0414.9-0840	J041433.10-084206.8	04:14:33.10	-08:42:06.86	2016-09-11	1200	30	?	bzb	w, N
3FGL J0420.4-6013	J042011.02-601505.5	04:20:11.03	-60:15:05.51	2015-08-23	600	38	?	bzb	w,x
3FGL J0437.7-7330	J043837.07-732921.6	04:38:37.07	-73:29:21.60	2016-08-30	600	24	0.150 ± 0.001	gal	S,w,M,x
3FGL J0704.3-4828	J070421.81-482647.5	07:04:21.82	-48:26:47.59	2016-12-22	1800	20	?	bzb	w,x
3FGL J0721.5-0221	J072113.90-022055.0	07:21:13.90	-02:20:55.07	2014-12-17	1800	28	?	bzb	N,w,x
3FGL J0747.5-4927	J074724.74-492633.1	07:47:24.74	-49:26:33.18	2016-12-30	1800	36	?	bzb	S,w
3FGL J0826.3-6400	J082627.86-640415.4	08:26:27.87	-64:04:15.45	2017-01-30	1800	51	?	bzb	S,w,x
3FGL J1013.4-4008	J101319.30-400550.4	10:13:19.50	-40:05:49.20	2017-01-30	2400	100	?	bzb	S,N,w
3FGL J1033.0-5945	J103332.15-503528.8	10:33:32.16	-50:35:28.82	2016-12-22	1200	27	?	bzb	w,x
3FGL J1100.2-2044	J110028.22-205000.7	11:00:28.32	-20:50:05.60	2017-01-30	1000	33	0.239 ± 0.001	gal	N,w,s
3FGL J1132.0-4736	J113209.26-473853.3	11:32:09.26	-47:38:53.31	2017-01-30	600	41	0.210 ± 0.001	gal	S,w,M,x
3FGL J1325.2-5411	J132457.35-541503.2	13:24:57.36	-54:15:03.29	2016-08-02	900	20	0.218 ± 0.001	gal	w
3FGL J1946.4-5403	J194633.62-540236.4	19:46:33.63	-54:02:36.43	2015-06-23	900	35	0.460 ± 0.002	qso	w
3FGL J2009.2-1458	J200838.59-150453.2	20:08:38.60	-15:04:53.27	2015-08-23	600	10	0.990 ± 0.004	qso	N,w
3FGL J2030.5-1439	J203027.91-143917.1	20:30:27.91	-14:39:17.17	2016-08-02	1200	25	0.234 ± 0.001	qso	N,w,s
3FGL J2112.5-3044	J211217.41-304655.3	21:12:17.41	-30:46:55.33	2015-08-18	900	26	0.216 ± 0.001	gal	w,x
3FGL J2144.6-5640	J214429.57-563849.0	21:44:29.57	-56:38:49.08	2016-08-02	1200	25	?	bzb	w,x
3FGL J2150.5-1754	J215046.60-174954.1	21:50:46.61	-17:49:54.18	2015-08-26	600	55	0.186 ± 0.001	gal	N,w
3FGL J2209.8-0450	J220941.69-045110.3	22:09:41.70	-04:51:10.33	2015-08-23	600	54	?	bzb	F,N,w,s
3FGL J2237.5-8326	J224201.61-832744.4	22:42:01.62	-83:27:44.45	2015-08-18	900	50	0.202 ± 0.001	qso	w
3FGL J2244.6+2503	J224436.66+250343.1	22:44:36.67	+25:03:43.20	2015-08-18	600	36	?	bzb	N,w,s
3FGL J2300.1-3547	J230053.29-355051.0	23:00:53.30	-35:50:51.08	2016-12-30	1200	49	0.753 ± 0.001	qso	w
3FGL J2321.6-1619	J232136.98-161928.3	23:21:36.98	-16:19:28.32	2015-08-23	600	47	?	bzb	N,w
3FGL J2337.2-8425	J233627.96-842652.1	23:36:27.97	-84:26:52.17	2015-08-18	600	22	?	bzb	w
3FGL J2351.9-7601	J235116.13-760015.5	23:51:16.13	-76:00:15.53	2015-08-26	600	40	?	bzb	S,w,x
3FGL J2358.6-1809	J235836.83-180717.4	23:58:36.84	-18:07:17.48	2015-08-23	600	51	?	bzb	N,w,x
1FGL J1129.2-0528	J112914.05-052856.3	11:29:14.06	-05:28:56.36	2015-05-20	1350	34	0.920 ± 0.001	qso	F,N,w,s

UGSS

Table 1 : Observing Log and Summary of Results

Fermi Name	WISE Counterpart	R.A. (J2000) hh:mm:ss	Dec. (J2000) dd:mm:ss	Obs. Date yy-mm-dd	Exp. Time (s)	S/N	z	Class	Notes
BCUs AND AGUs									
3FGL J0127.2+0325	J012713.94+032300.6	01:27:13.95	+03:23:00.64	2016-12-22	1800	44	?	bzb	N,w,s,x
3FGL J0310.4-5015	J031034.72-501631.1	03:10:34.72	-50:16:31.13	2014-12-17	2100	62	?	bzb	S,w,X,x
3FGL J0439.9-1859	J043949.72-190101.5	04:39:49.73	-19:01:01.57	2014-12-17	2100	57	?	bzb	Pm,w,x
3FGL J0626.6-4259	J062636.71-425805.9	06:26:36.71	-42:58:05.92	2017-01-30	900	45	?	bzb	w,X
3FGL J0649.6-3138	J064933.60-313920.3	06:49:33.60	-31:39:20.34	2014-12-18	1050	55	≥ 0.563	bzb	w,X,x
3FGL J0703.4-3914	J070312.65-391418.8	07:03:12.66	-39:14:18.89	2014-12-17	1800	49	?	bzb	w, S,N,A,X,x
3FGL J0803.3-0339	J080311.45-033554.5	08:03:11.45	-03:35:54.57	2014-12-18	900	45	0.365 ± 0.001	bzq	Pm,V,T N,w,x
3FGL J0827.2-0711	J082706.16-070845.9	08:27:06.17	-07:08:45.93	2015-05-19	300	52	?	bzb	Pm,N,w,M,X
3FGL J0858.1-3130	J085802.90-313038.3	08:58:02.91	-31:30:38.31	2014-12-18	1050	25	?	bzb	w,X
3FGL J0947.1-2542	J094709.52-254059.9	09:47:09.53	-25:40:59.97	2014-12-18	600	95	?	bzb	N,w,6,X,x
3FGL J1009.0-3137	J100850.54-313905.5	10:08:50.55	-31:39:05.50	2015-05-19	1350	98	0.534 ± 0.001	bzb	Pm,T,S,N,c,w
3FGL J1106.4-3643	J110624.04-364658.9	11:06:24.04	-36:46:58.96	2015-05-21	1500	62	1.084 ± 0.001	bzb	Pm,N,S,A,c,w
3FGL J1125.0-2101	J112508.62-210105.9	11:25:08.63	-21:01:05.98	2015-05-19	1200	103	?	bzb	Pm,N,c,w,X,
3FGL J1203.5-3925	J120317.88-392620.9	12:03:17.89	-39:26:20.96	2015-05-20	900	63	0.227 ± 0.001	bzb	Pm,S,N,c,w
3FGL J1218.8-4827	J121902.26-482627.9	12:19:02.27	-48:26:27.98	2015-05-21	1800	84	?	bzb	Pm,S,c,w
3FGL J1307.6-4300	J130737.98-425938.9	13:07:37.98	-42:59:38.97	2015-05-19	600	115	?	bzb	w,X,x
3FGL J1312.7-2349	J131248.76-235047.3	13:12:48.76	-23:50:47.38	2015-05-19	1800	63	≥ 0.462	bzb	N,w
3FGL J1512.2-2255	J151212.75-225508.4	15:12:12.76	-22:55:08.47	2015-05-21	2700	67	?	bzb	w,X,x
3FGL J1518.0-2732	J151803.59-273131.1	15:18:03.60	-27:31:31.13	2015-05-20	150	67	?	bzb	Pm,T,N,A,c,w,M,g
3FGL J1539.8-1128	J153941.19-112835.3	15:39:41.20	-11:28:35.36	2015-05-20	600	107	?	bzb	Pm,N,w,6,g,X,
3FGL J1547.1-2801	J154712.13-280221.5	15:47:12.13	-28:02:21.57	2015-05-20	1350	54	?	bzb	w,X
3FGL J1617.4-5846	J161717.91-584808.0	16:17:17.91	-58:48:08.07	2015-05-20	900	115	1.414 ± 0.001	bzq	Pm,A,w,X
3FGL J1637.6-3449	NVSS J163750-344915	16:37:50.99	-34:49:15.40	2015-05-19	300	62	?	bzb	N,A,X
3FGL J1656.8-2010	J165655.14-201056.2	16:56:55.15	-20:10:56.30	2015-05-21	1800	43	?	bzb	w,X
3FGL J1955.0-1605	J195500.65-160338.4	19:55:00.66	-16:03:38.41	2015-05-19	1200	65	≥ 0.630	bzb	w,N,6,g,X
3FGL J2024.4-0848	J202429.37-084804.6	20:24:29.37	-08:48:04.66	2015-05-19	1800	43	?	bzb	N,w,6,g,X
2FGL J1922.6-7454	J192243.02-745349.5	19:22:43.02	-74:53:49.60	2015-08-26	600	31	?	bzb	S,w,X
KNOWN BLAZARS									
3FGL J0814.1-1012	J081411.69-101210.2	08:14:11.69	-10:12:10.25	2014-12-18	600	93	?	bzb	N,A,6,w,x

Column description: (1) 3FGL name; (2) Associated counterpart; (3) R.A. (Equinox J2000); (4) Dec. (Equinox J2000); (5) Observation date; (6) Exposure time; (7) Signal-to-noise ratio; (8) redshift, question marks indicate unknown z; (9) Source classification; (10) Multifrequency notes: V, VLA Low-frequency Sky Survey

Discrete Source Catalog (VLSS) (Cohen et al. 2007); Pm, Parkes-MIT-NRAO Surveys (PMN) (Wright et al. 1994); T, Texas Survey of Radio Sources (TEXAS) (Douglas et al. 1996); c, Combined Radio All-Sky Targeted Eight-GHz Survey (CRATES) (Healey et al. 2007); N, NRAO VLA Sky Survey (NVSS) (Condon et al. 1998); F, VLA Faint Images of The Radio Sky at 20 cm (FIRST) (Becker et al. 1995); w, WISE all-sky survey in the Allwise Source catalog Two (WISE) (Wright et al. 2010); M, Two Micron All Sky Survey (2MASS) (Skrutskie et al. 2006); s, Sloan Digital Sky Survey Data Release 9 (SDSS DR9) (Ahn et al. 2012); 6, Six-degree-field Galaxy Redshift Survey (6dFGS) (Jones et al. 2004; Jones et al. 2009); **g**, **GALaxy Evolution eXplorer All-Sky Survey Source Catalog (GALEX)** (Seibert et al. 2012); X, ROSAT Bright Source Catalog (RBSC) (Voges, W. 1999); X, ROSAT Faint Source Catalog (RFSC) (Voges, W. 2000); x, XMM-Newton Slew Survey (XMMSL) (Saxton et al. 2008; Warwick et al. 2012); x, Deep *Swift* X-Ray Telescope Point Source Catalog (1SXPS) (Evans et al. 2014); x, Chandra Source Catalog (CSC) (Evans et al. 2010).

5 Summary and Conclusions

We present the spectroscopic observations of **61** optical targets associated with Fermi-LAT detected sources. The observations were taken between 2014-2017 as part of our follow up optical campaign. Our sample consist of **33** blazar-like sources lying within the positional uncertainty regions of UGSs, selected on the basis of their IR colors, **27** BCUs and 1 known 3FGL BL Lac object. Results are summarized as follows.

- For the UGSs, we classified **20** candidates counterparts as BZBs. An estimate of redshift for WISE J012152.69-391544.2 potential counterpart of the source at 3FGL J0121.8-3917 ($z = 0.390$). The remaining targets are thought to be contaminants of the WISE procedure used to search for potential counterparts (D’Abrusco et al. 2013; Massaro et al. 2013a; Massaro et al. 2013b), there are 7 QSOs, without radio information, and 6 galaxies.
- We confirm the blazar nature of all the **27** BCUs. Two of them are BZQs: WISE J080311.45-033554.5 counterpart of 3FGL J0803.3-0339 and WISE J161717.91-584808.0 counterpart of 3FGL J1617.4-5846 at $z = 0.365$ and $z = 1.414$, respectively. All the others are classified as BZBs with emission or absorption lines in their optical spectra with $EW < 5 \text{ \AA}$. For this subsample of BZBs we obtained 6 redshifts estimates.

We observed again 3FGL J0814.1-1012, previously observed and classified by Álvarez Crespo et al. (2016b). We confirm the blazar nature of its associated counterpart WISE J081411.69-101210.2. The spectrum shows a featureless blue continuum as a classical BZB.

To summarize, we identified 50 new blazars, correspondent to an additional 20 % of those already classified and confirmed during our campaign to date. Finally, we also highlight the discovery of the BZB with the second most distant BL Lac known to date, 3FGL J1106.4-3643, with $z \geq 1.084$ estimated from the Mg II absorption lines.

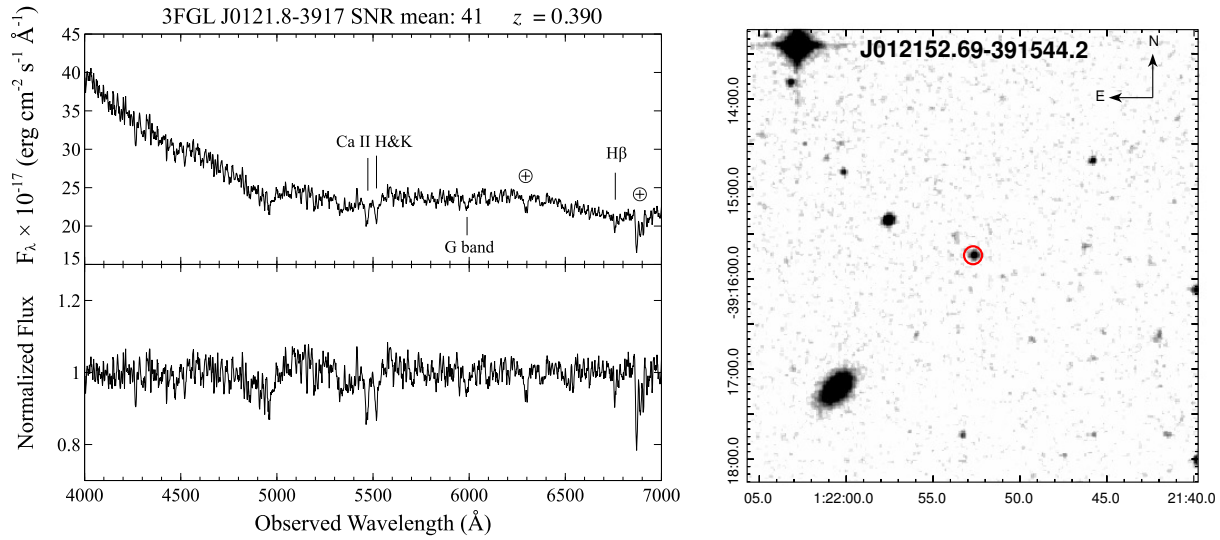


Fig. 2 (Left panel) Optical spectrum of WISE J012152.69-391544.2 associated with 3FGL J0121.8-3917. Signal-to-noise ratio is reported in the Figure. (Right panel) The finding chart ($5' \times 5'$) retrieved from the Digital Sky Survey highlighting the location of the potential source: WISE J012152.69-391544.2 (red circle).

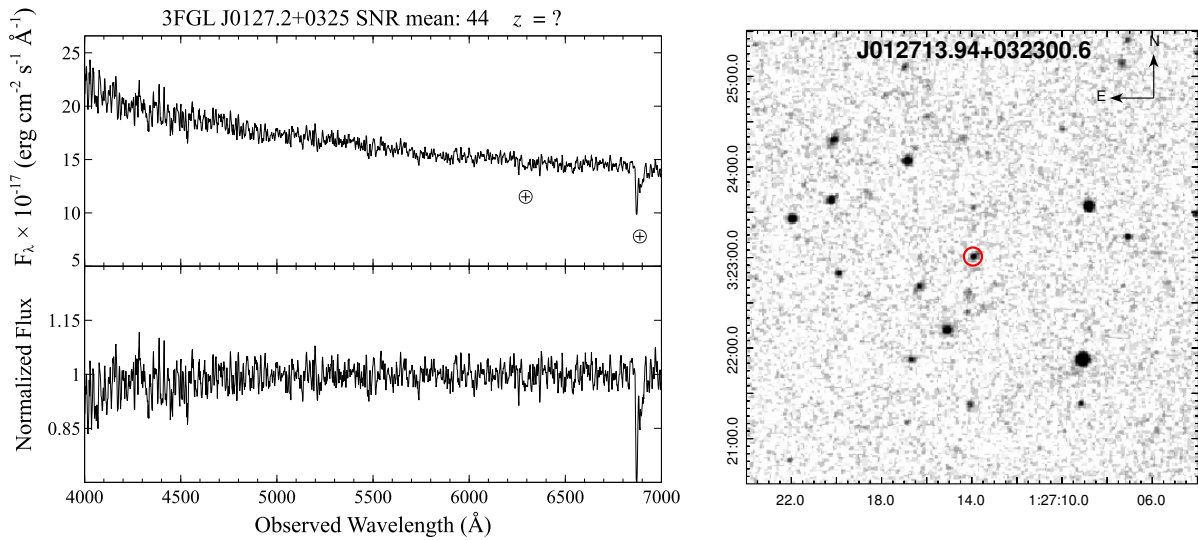


Fig. 3 (Left panel) Optical spectrum of WISE J012713.94+032300.6 associated with 3FGL J0127.2+0325, in the upper part it is shown the Signal-to-Noise Ratio of the spectrum. (Right panel) The finding chart ($5' \times 5'$) retrieved from the Digital Sky Survey highlighting the location of the counterpart: WISE J012713.94+032300.6 (red circle).

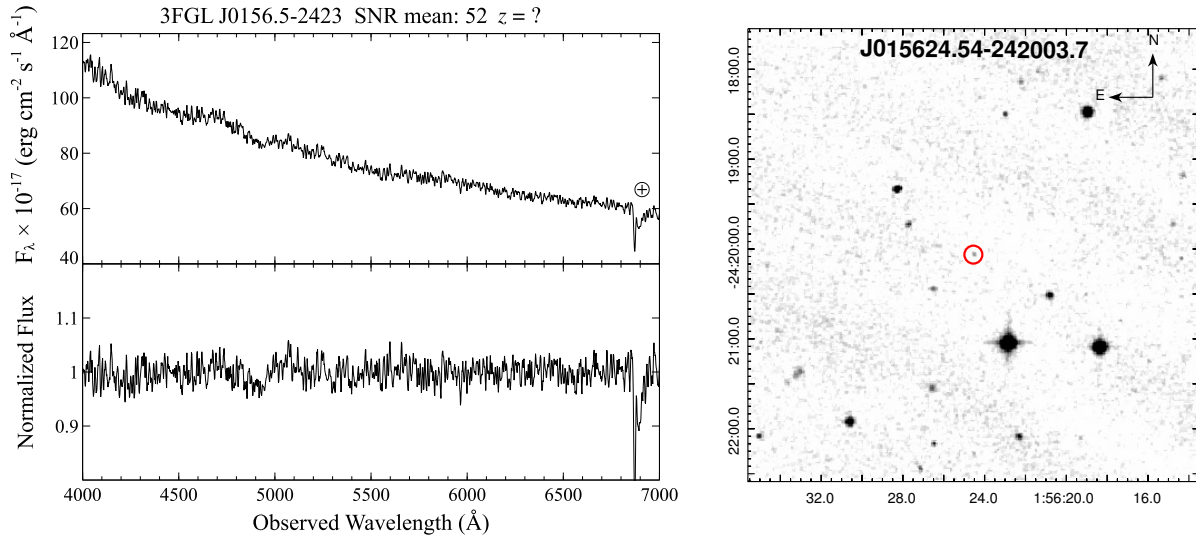


Fig. 4 (Left panel) Optical spectrum of WISE J015624.54-242003.7 associated with 3FGL J0156.5-2423, in the upper part it is shown the Signal-to-Noise Ratio of the spectrum. (Right panel) The finding chart ($5' \times 5'$) retrieved from the Digital Sky Survey highlighting the location of the counterpart: WISE J015624.54-242003.7 (red circle).

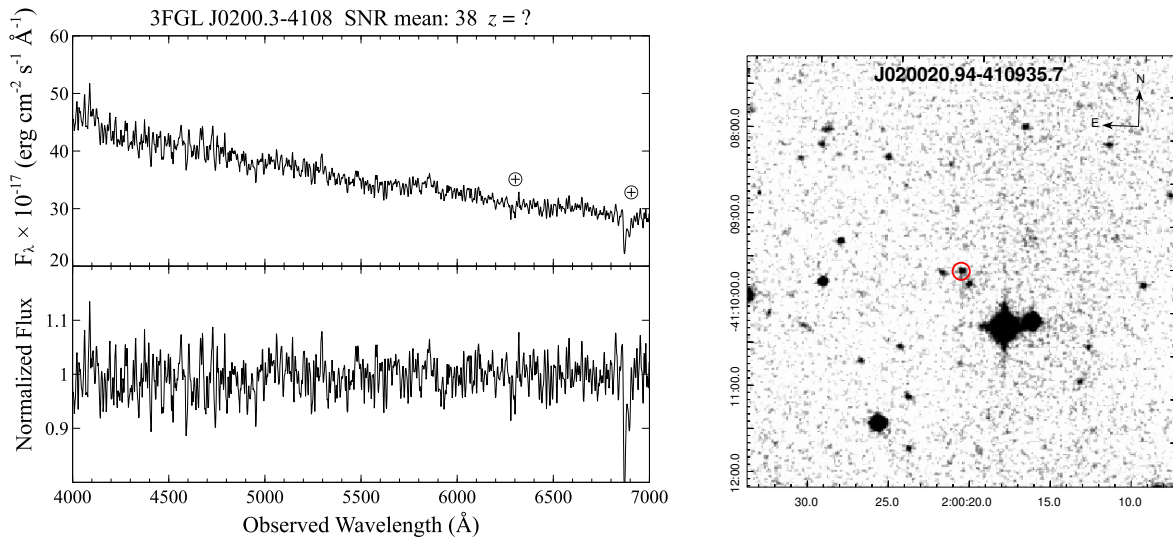


Fig. 5 (Left panel) Optical spectrum of WISE J020020.94-410935.7 associated with 3FGL J0200.3-4108. Signal-to-noise ratio is reported in the Figure. (Right panel) The finding chart ($5' \times 5'$) retrieved from the Digital Sky Survey highlighting the location of the potential source: WISE J020020.94-410935.7 (red circle).

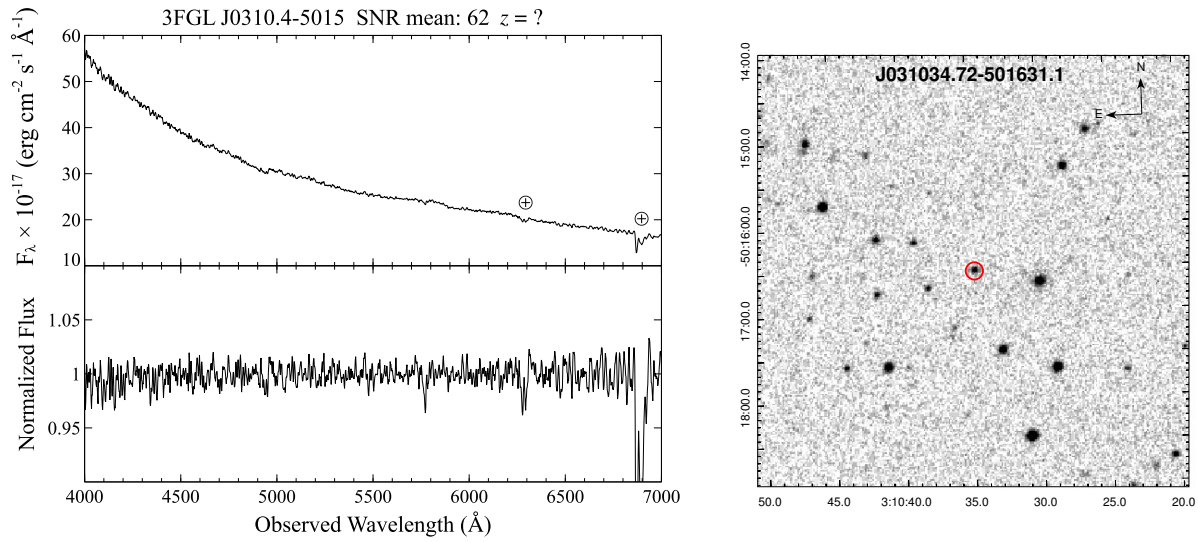


Fig. 6 (Left panel) Optical spectrum of WISE J031034.72-501631.1, associated with 3FGL J0310.4-5015. Signal-to-noise ratio is reported in the Figure. (Right panel) The finding chart ($5' \times 5'$) retrieved from the Digital Sky Survey highlighting the location of the potential source: WISE J031034.72-501631.1 (red circle).

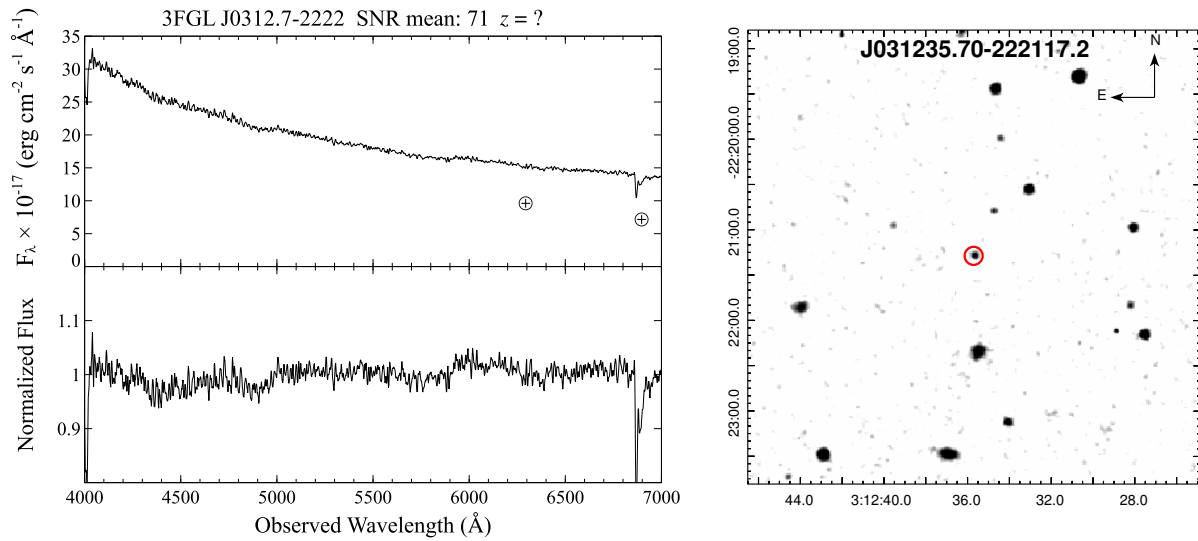


Fig. 7 (Left panel) Optical spectrum of WISE J031235.70-222117.2 associated with 3FGL J0312.7-2222. Signal-to-noise ratio is reported in the Figure. (Right panel) The finding chart ($5' \times 5'$) retrieved from the Digital Sky Survey highlighting the location of the potential source: WISE J031235.70-222117.2 (red circle).

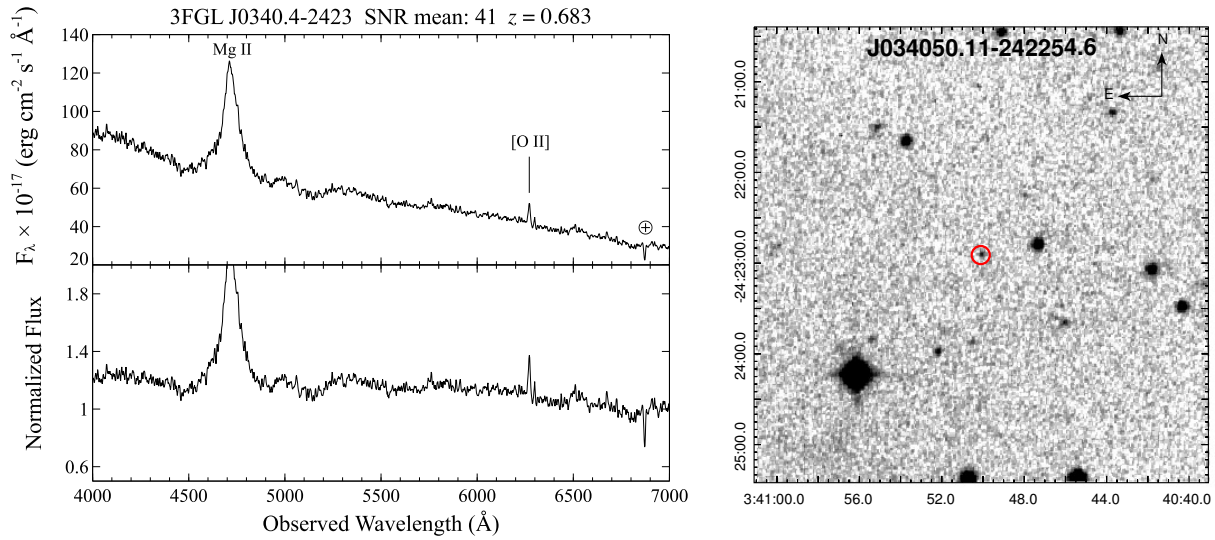


Fig. 8 (Left panel) Optical spectrum of WISE J034050.11-242254.6 associated with 3FGL J0340.4-2423. Signal-to-noise ratio is reported in the Figure. (Right panel) The finding chart (5' × 5') retrieved from the Digital Sky Survey highlighting the location of the potential source: WISE J034050.11-242254.6 (red circle).

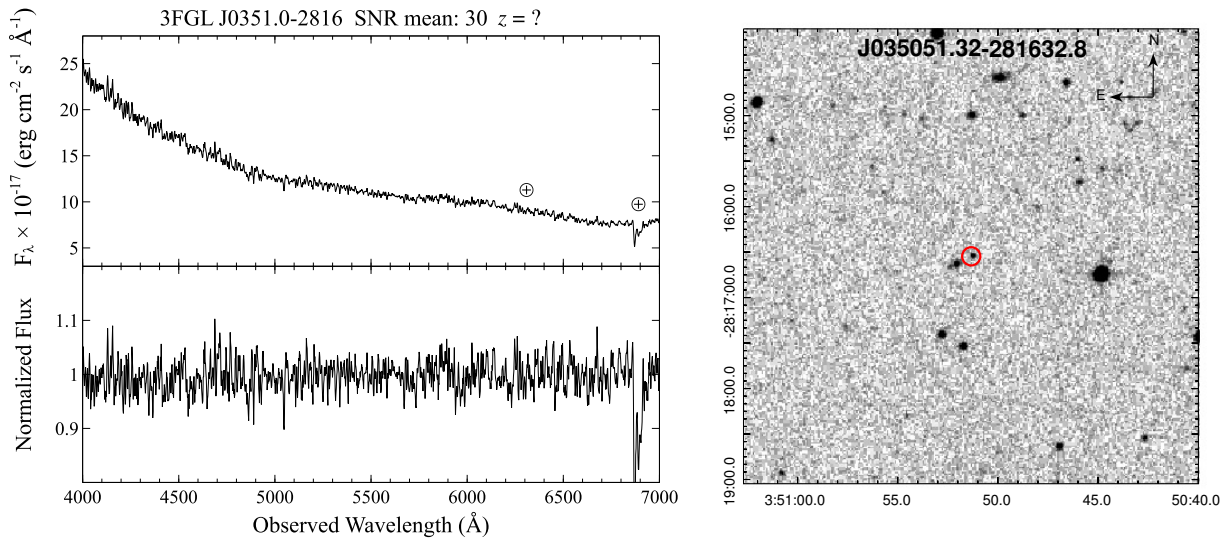


Fig. 9 (Left panel) Optical spectrum of WISE J035051.32-281632.8 associated with 3FGL J0351.0-2816. Signal-to-noise ratio is reported in the Figure. (Right panel) The finding chart (5' × 5') retrieved from the Digital Sky Survey highlighting the location of the potential source: WISE J035051.32-281632.8 (red circle).

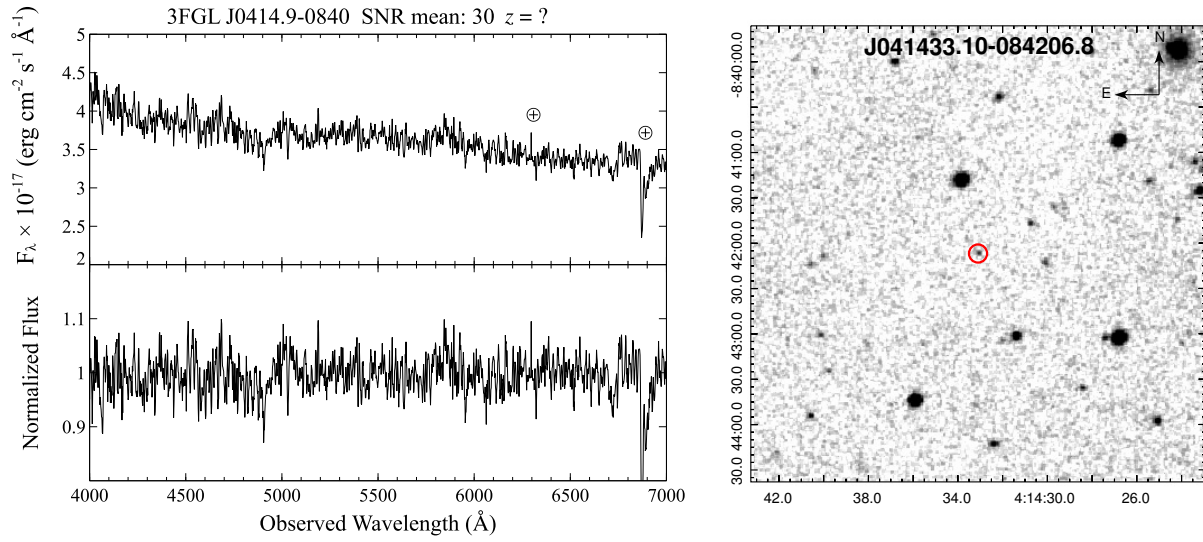


Fig. 10 (Left panel) Optical spectrum of WISE J041433.10-084206.8, associated with 3FGL J0414.9-0840. Signal-to-noise ratio is reported in the Figure. (Right panel) The finding chart ($5' \times 5'$) retrieved from the Digital Sky Survey highlighting the location of the potential source: WISE J041433.10-084206.8 (red circle).

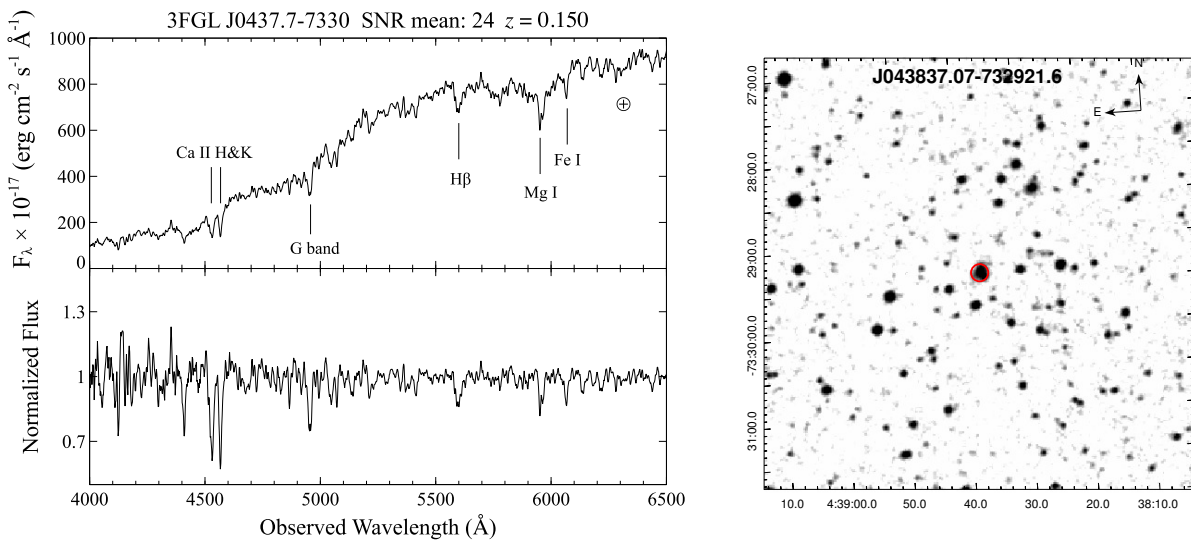


Fig. 11 (Left panel) Optical spectrum of WISE J043837.07-732921.6, associated with 3FGL J0437.7-7330. Signal-to-noise ratio is reported in the Figure. (Right panel) The finding chart ($5' \times 5'$) retrieved from the Digital Sky Survey highlighting the location of the potential source: WISE J043837.07-732921.6 (red circle).

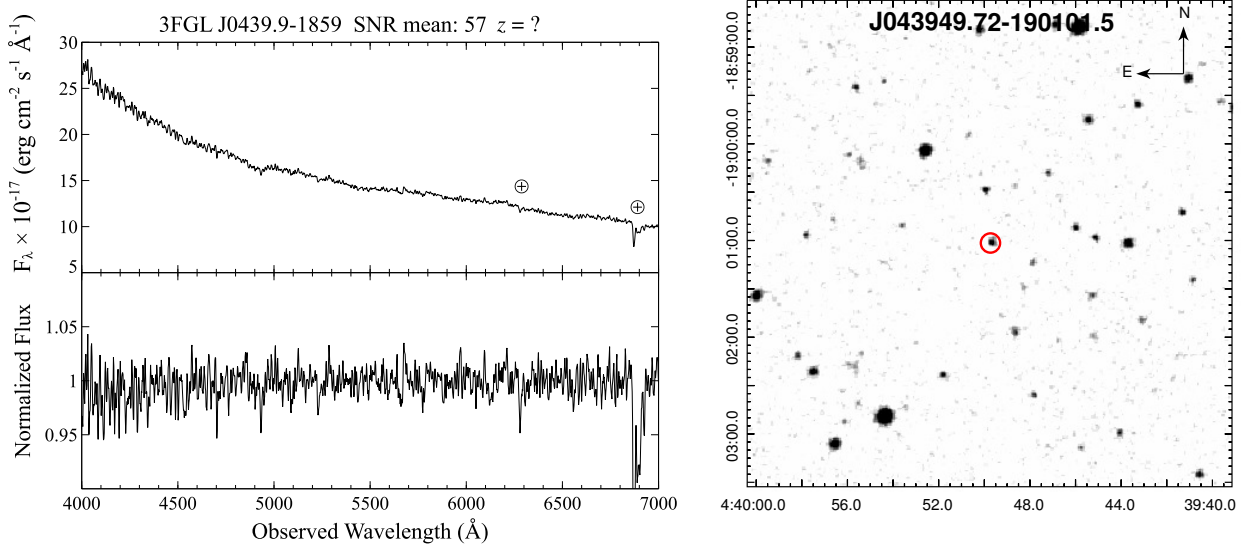


Fig. 12 (Left panel) Optical spectrum of WISE J043949.72-190101.5 associated with 3FGL J0439.9-1859, in the upper part it is shown the Signal-to-Noise Ratio of the spectrum. (Right panel) The finding chart (5' × 5') retrieved from the Digital Sky Survey highlighting the location of the counterpart: WISE J043949.72-190101.5 (red circle).

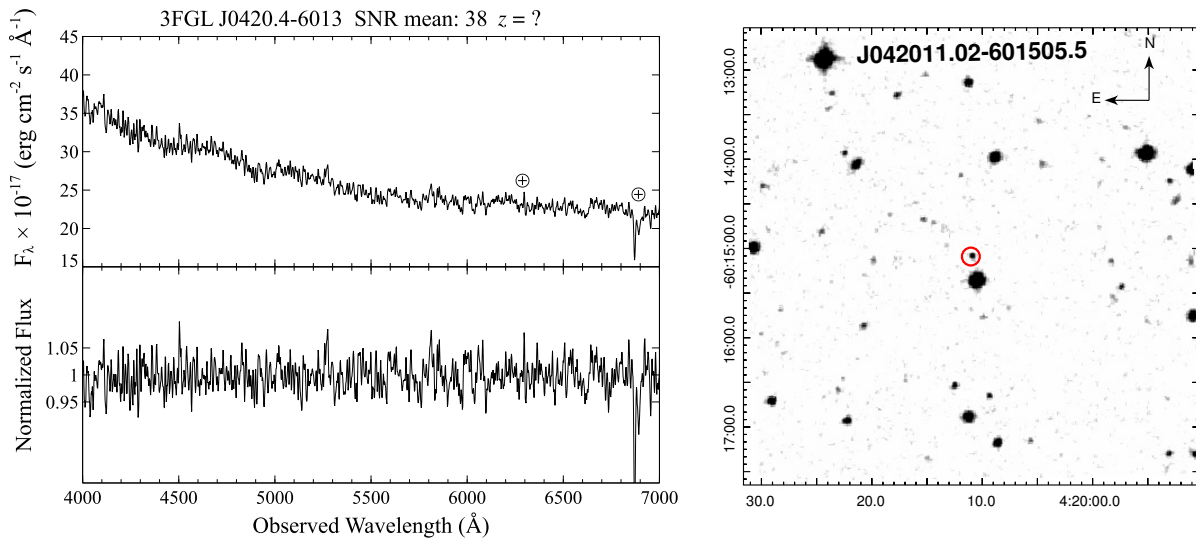


Fig. 13 (Left panel) Optical spectrum of WISE J042011.02-601505.5, associated with 3FGL J0420.4-6013. Signal-to-noise ratio is reported in the Figure. (Right panel) The finding chart (5' × 5') retrieved from the Digital Sky Survey highlighting the location of the potential source: WISE J042011.02-601505.5 (red circle).

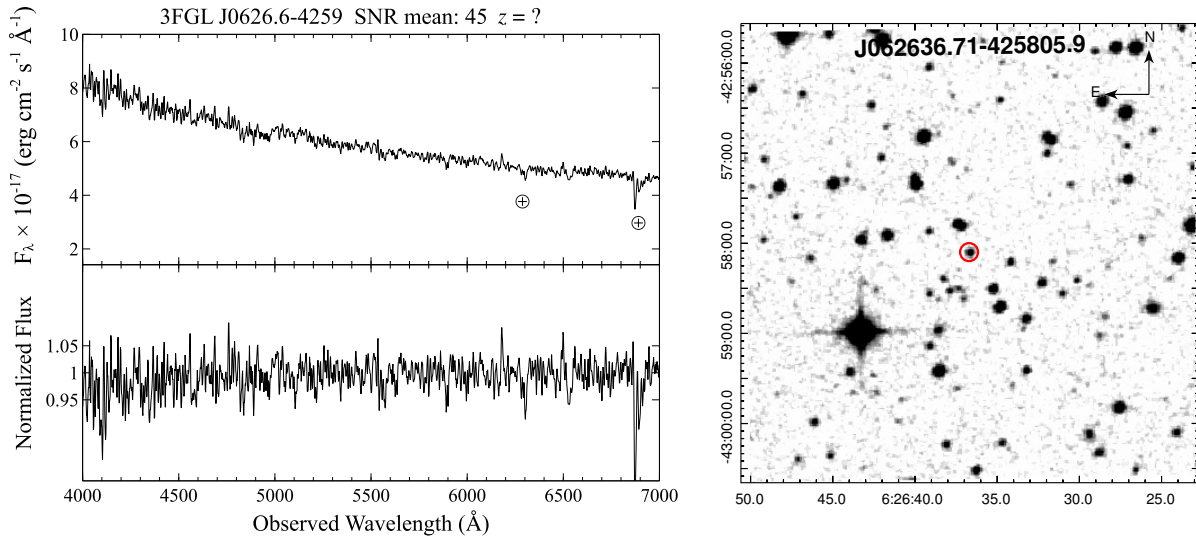


Fig. 14 (Left panel) Optical spectrum of WISE J062636.71-425805.9 associated with 3FGL J0626.6-4259, in the upper part it is shown the Signal-to-Noise Ratio of the spectrum. (Right panel) The finding chart ($5' \times 5'$) retrieved from the Digital Sky Survey highlighting the location of the counterpart: WISE J062636.71-425805.9 (red circle).

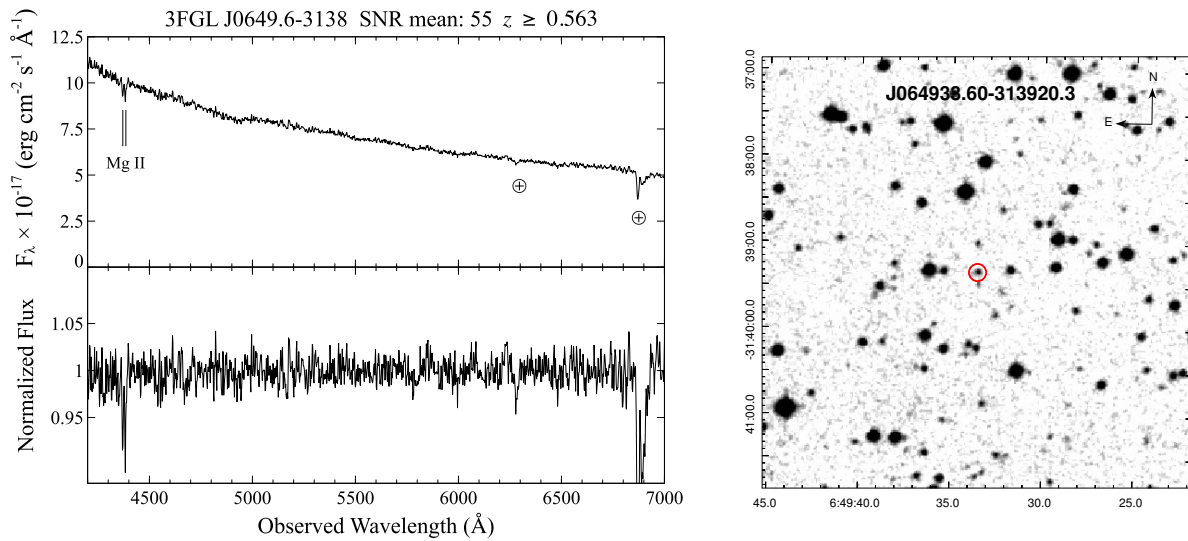


Fig. 15 (Left panel) Optical spectrum of WISE J064933.60-313920.3 associated with 3FGL J0649.6-3138, in the upper part it is shown the Signal-to-Noise Ratio of the spectrum. (Right panel) The finding chart ($5' \times 5'$) retrieved from the Digital Sky Survey highlighting the location of the counterpart: WISE J064933.60-313920.3 (red circle).

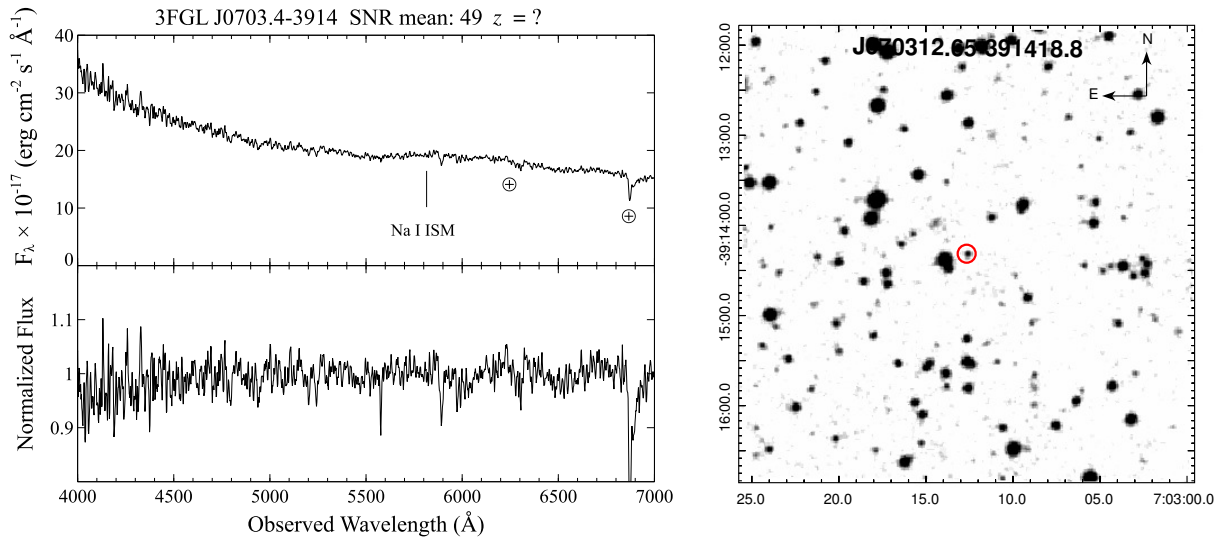


Fig. 16 (Left panel) Optical spectrum of WISE J070312.65-391418.8 associated with 3FGL J0703.4-3914, in the upper part it is shown the Signal-to-Noise Ratio of the spectrum. (Right panel) The finding chart ($5' \times 5'$) retrieved from the Digital Sky Survey highlighting the location of the counterpart: WISE J070312.65-391418.8 (red circle).

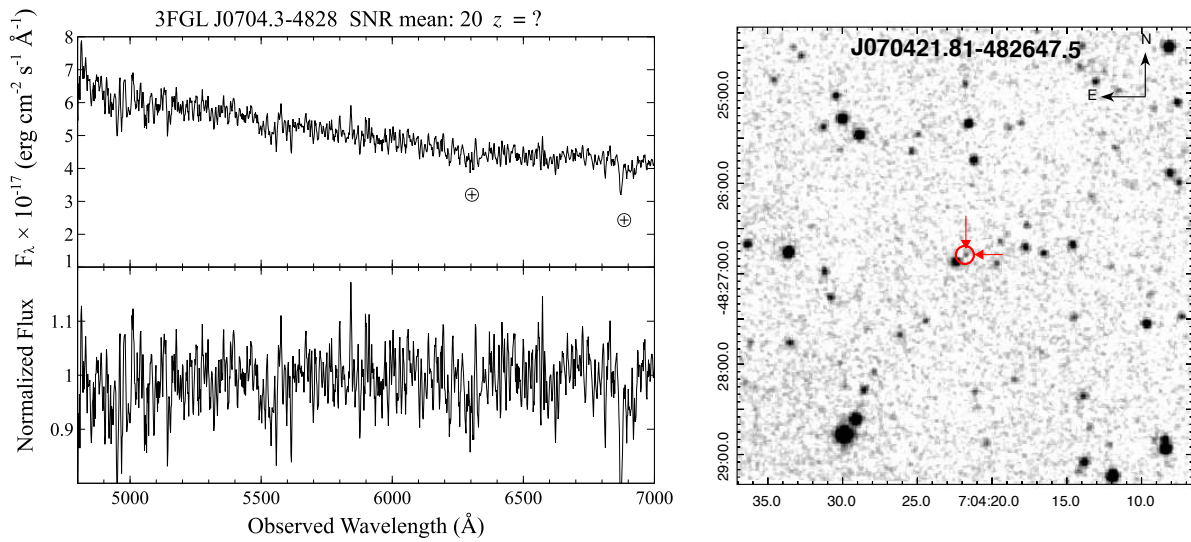


Fig. 17 (Left panel) Optical spectrum of WISE J070421.81-482647.5, associated with 3FGL J0704.3-4828. Signal-to-noise ratio is reported in the Figure. (Right panel) The finding chart ($5' \times 5'$) retrieved from the Digital Sky Survey highlighting the location of the potential source: WISE J070421.81-482647.5 (red circle).

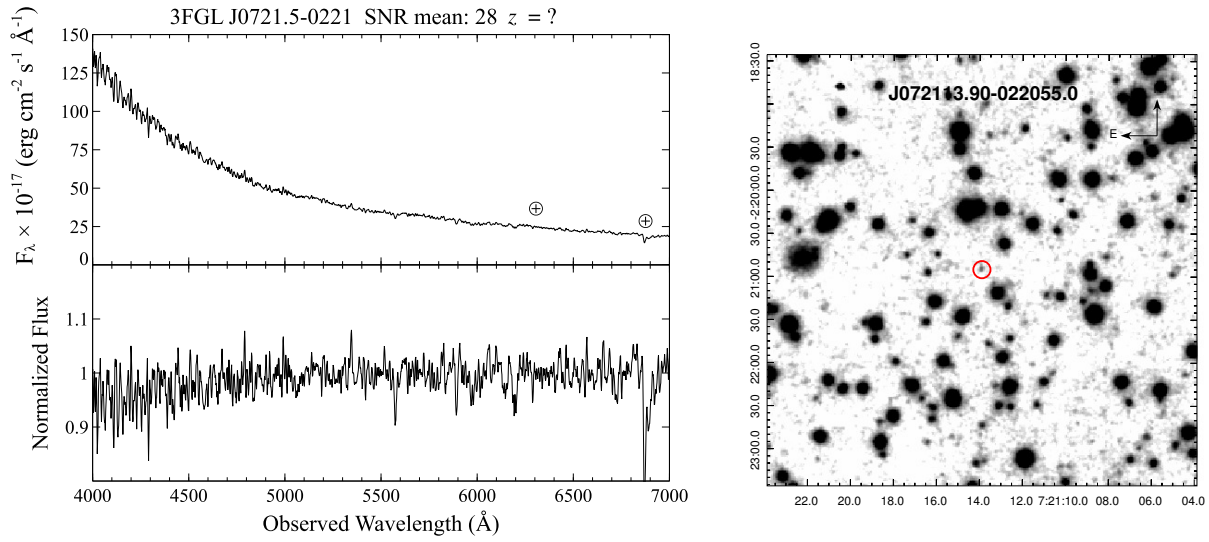


Fig. 18 (Left panel) Optical spectrum of WISE J072113.90-022055.0 associated with 3FGL J0721.5-0221. Signal-to-noise ratio is reported in the Figure. (Right panel) The finding chart ($5' \times 5'$) retrieved from the Digital Sky Survey highlighting the location of the potential source: WISE J072113.90-022055.0 (red circle).

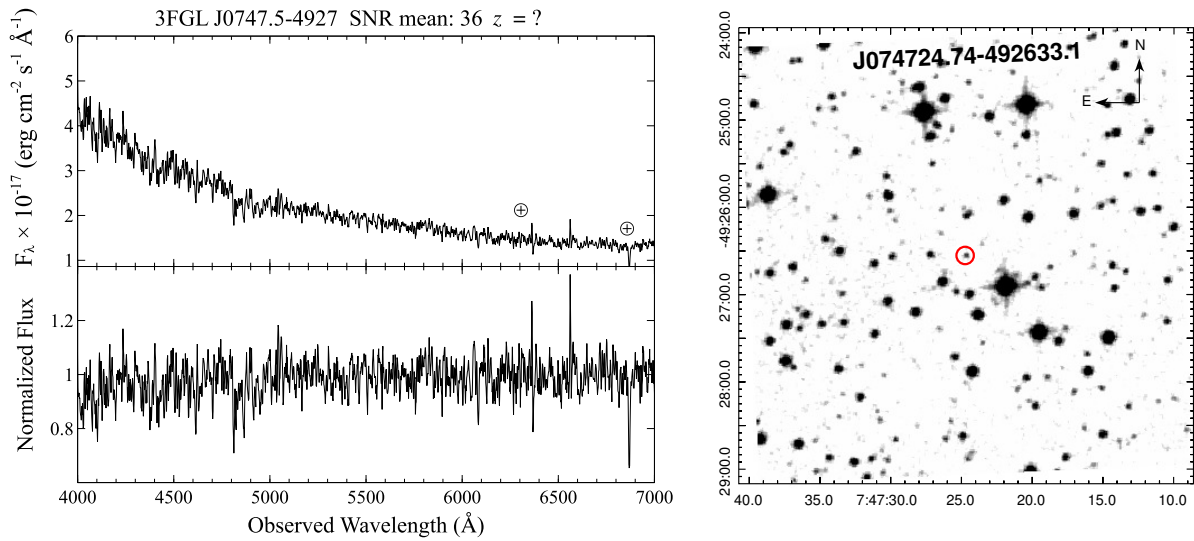


Fig. 19 (Left panel) Optical spectrum of WISE J074724.74-492633.1 associated with 3FGL J0747.5-4927. Signal-to-noise ratio is reported in the Figure. (Right panel) The finding chart ($5' \times 5'$) retrieved from the Digital Sky Survey highlighting the location of the potential source: WISE J074724.74-492633.1 (red circle).

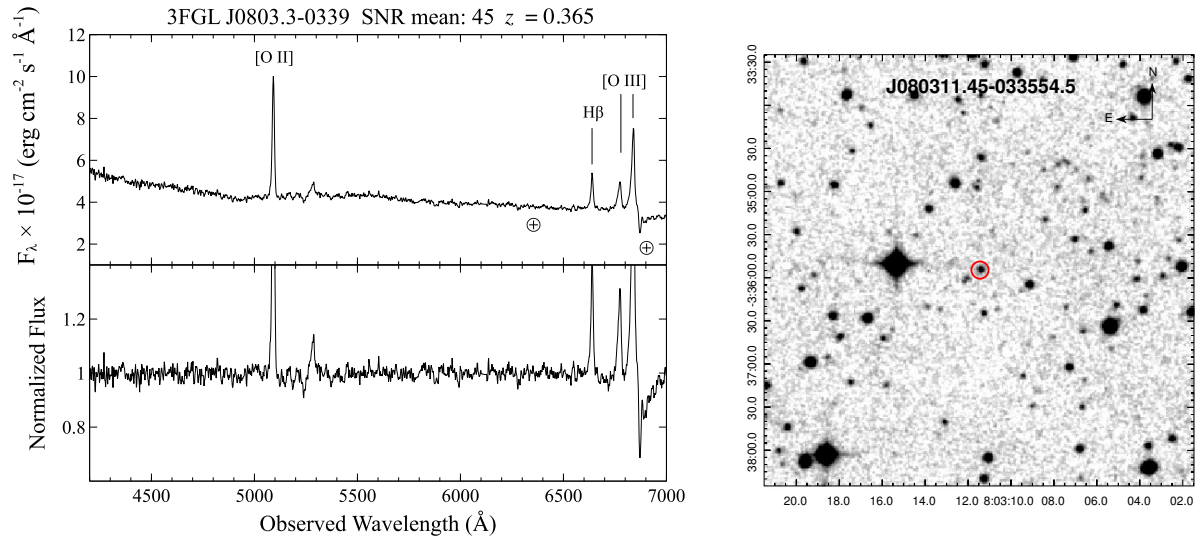


Fig. 20 (Left panel) Optical spectrum of WISE J080311.45-033554.5 associated with 3FGL J0803.3-0339. Signal-to-noise ratio is reported in the Figure. (Right panel) The finding chart ($5' \times 5'$) retrieved from the Digital Sky Survey highlighting the location of the counterpart: WISE J080311.45-033554.5 (red circle).

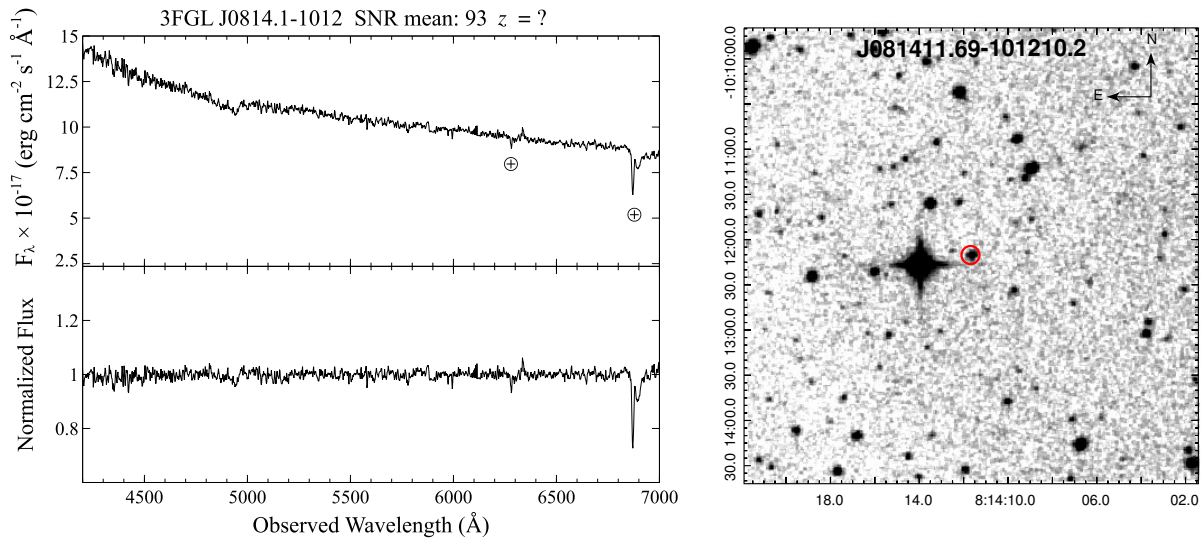


Fig. 21 (Left panel) Optical spectrum of WISE J081411.69-101210.2 associated with 3FGL J0814.1-1012, in the upper part it is shown the Signal-to-Noise Ratio of the spectrum. (Right panel) The finding chart ($5' \times 5'$) retrieved from the Digital Sky Survey highlighting the location of the counterpart: WISE J081411.69-101210.2 (red circle).

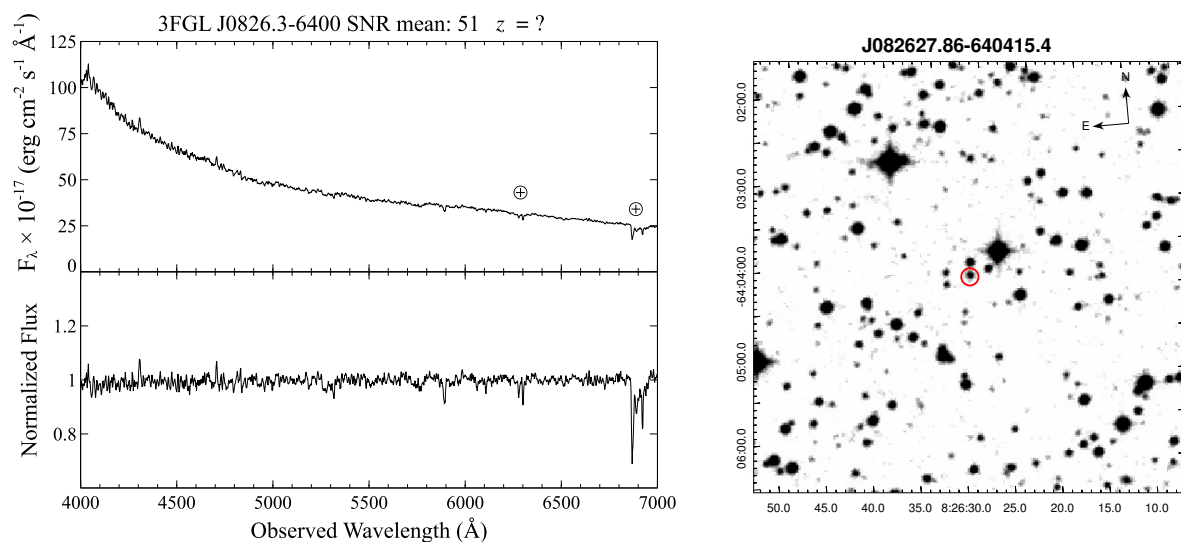


Fig. 22 (Left panel) Optical spectrum of WISE J082627.86-640415.4 associated with 3FGL J0826.3-6400. Signal-to-noise ratio is reported in the Figure. (Right panel) The finding chart ($5' \times 5'$) retrieved from the Digital Sky Survey highlighting the location of the potential source: WISE J082627.86-640415.4 (red circle).

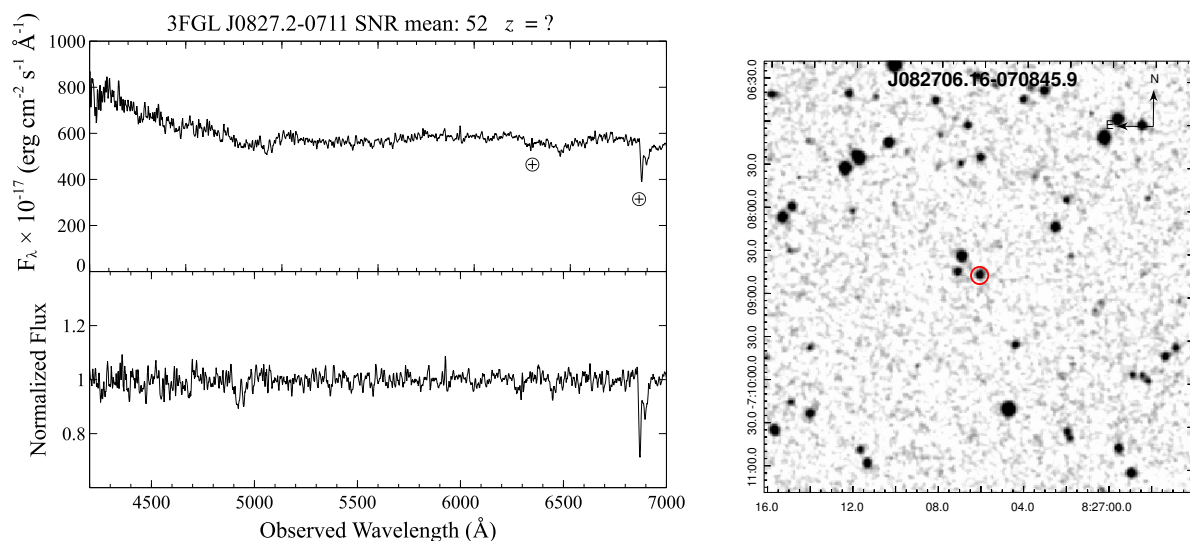


Fig. 23 (Left panel) Optical spectrum of WISE J082706.16-070845.9 associated with 3FGL J0827.2-0711, in the upper part it is shown the Signal-to-Noise Ratio of the spectrum. (Right panel) The finding chart ($5' \times 5'$) retrieved from the Digital Sky Survey highlighting the location of the counterpart: WISE J082706.16-070845.9 (red circle).

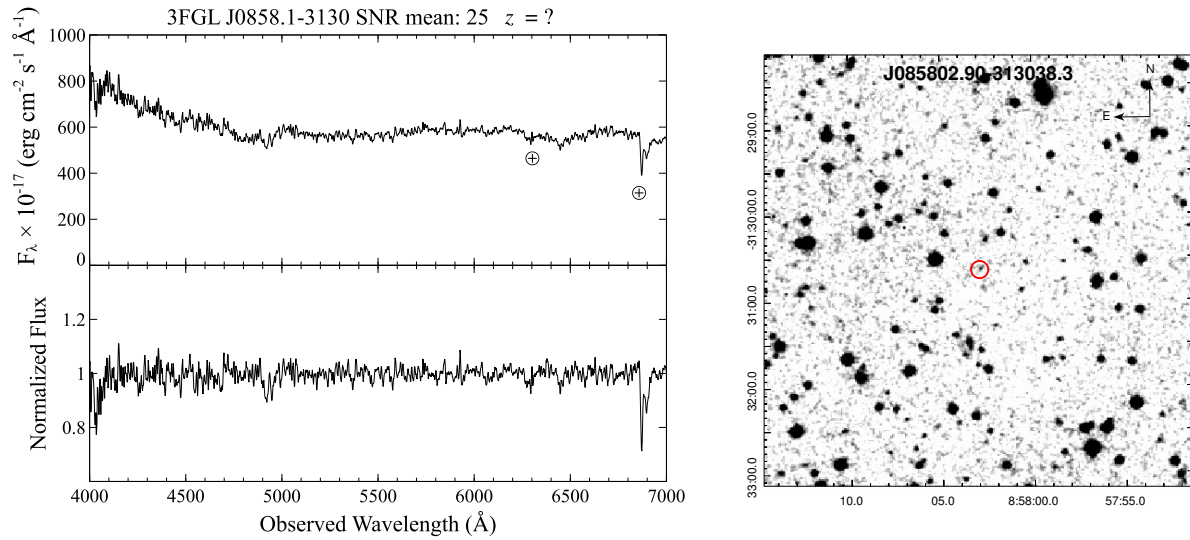


Fig. 24 (Left panel) Optical spectrum of WISE J085802.90-313038.3 associated with 3FGL J0858.1-3130, in the upper part it is shown the Signal-to-Noise Ratio of the spectrum. (Right panel) The finding chart ($5' \times 5'$) retrieved from the Digital Sky Survey highlighting the location of the counterpart: WISE J085802.90-313038.3 (red circle).

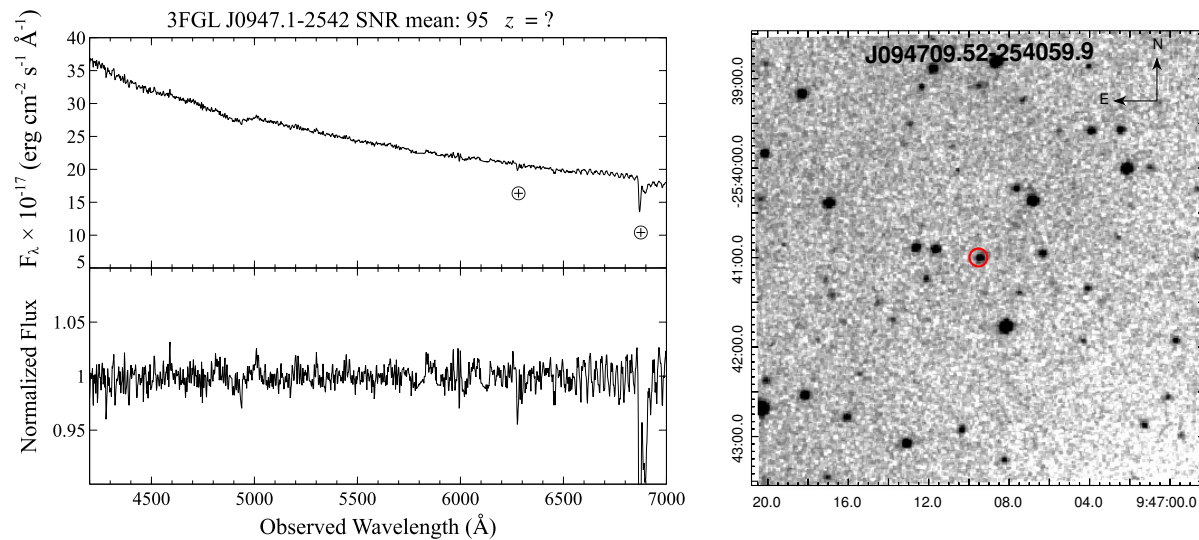


Fig. 25 (Left panel) Optical spectrum of WISE J094709.52-254059.9 associated with 3FGL J0947.1-2542, in the upper part it is shown the Signal-to-Noise Ratio of the spectrum. (Right panel) The finding chart ($5' \times 5'$) retrieved from the Digital Sky Survey highlighting the location of the counterpart: WISE J094709.52-254059.9 (red circle).

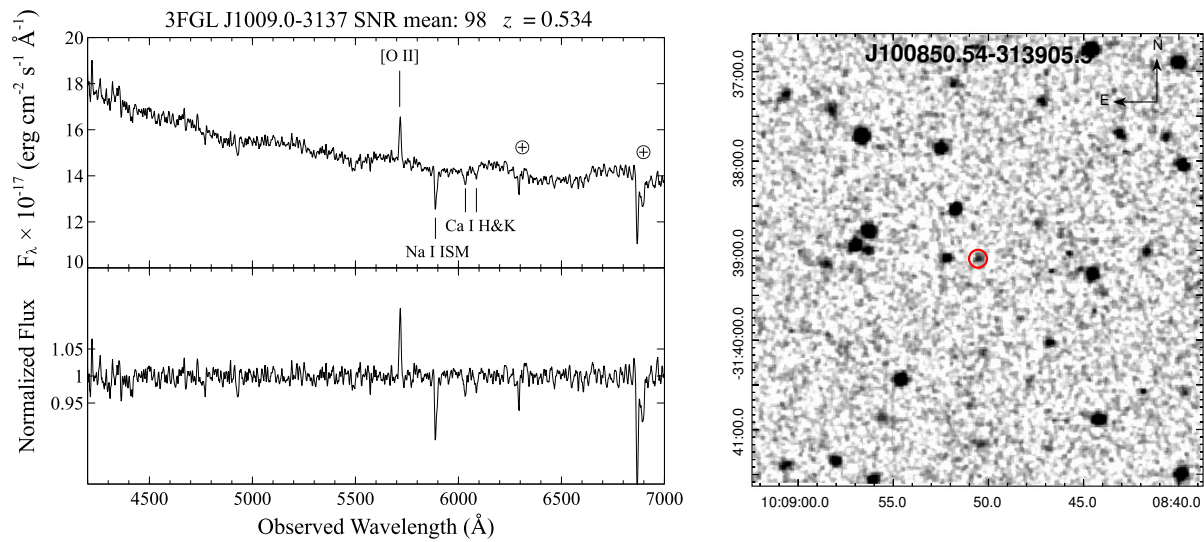


Fig. 26 (Left panel) Optical spectrum of WISE J100850.54-313905.5 associated with 3FGL J1009.0-3137, in the upper part it is shown the Signal-to-Noise Ratio of the spectrum. (Right panel) The finding chart ($5' \times 5'$) retrieved from the Digital Sky Survey highlighting the location of the counterpart: WISE J100850.54-313905.5 (red circle).

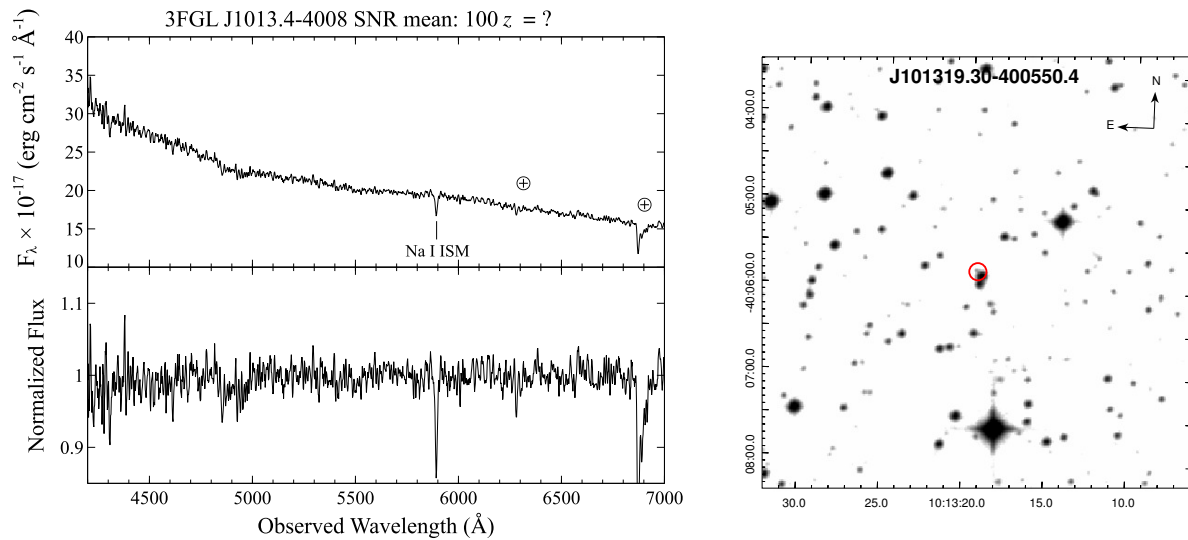


Fig. 27 (Left panel) Optical spectrum of WISE J101319.30-400550.4 associated with 3FGL J1013.4-4008. Signal-to-noise ratio is reported in the Figure. (Right panel) The finding chart ($5' \times 5'$) retrieved from the Digital Sky Survey highlighting the location of the potential source: WISE J101319.30-400550.4 (red circle).

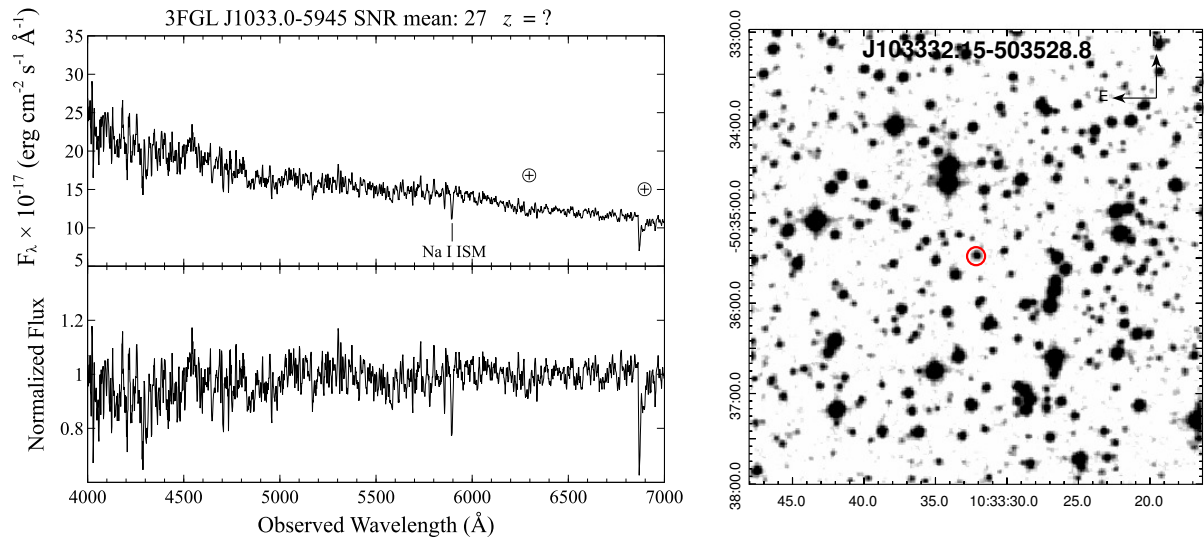


Fig. 28 (Left panel) Optical spectrum of WISE J103332.15-503528.8 associated with 3FGL J1033.0-5945, in the upper part it is shown the Signal-to-Noise Ratio of the spectrum. (Right panel) The finding chart ($5' \times 5'$) retrieved from the Digital Sky Survey highlighting the location of the counterpart: WISE J103332.15-503528.8 (red circle).

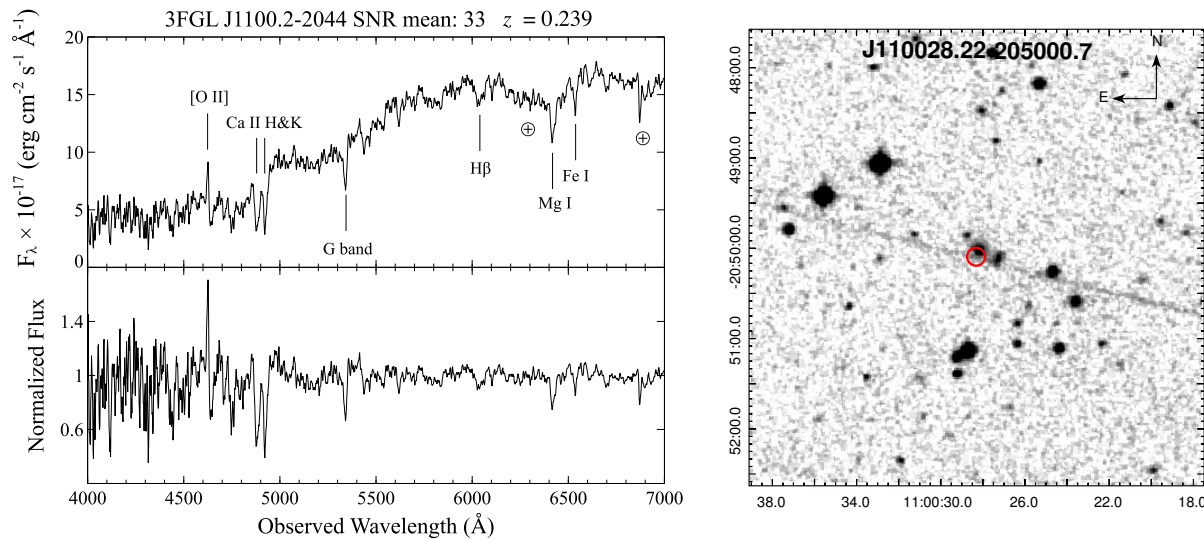


Fig. 29 (Left panel) Optical spectrum of WISE J110028.22-205000.7 associated with 3FGL J1100.2-2044. Signal-to-noise ratio is reported in the Figure. (Right panel) The finding chart ($5' \times 5'$) retrieved from the Digital Sky Survey highlighting the location of the potential source: WISE J110028.22-205000.7 (red circle).

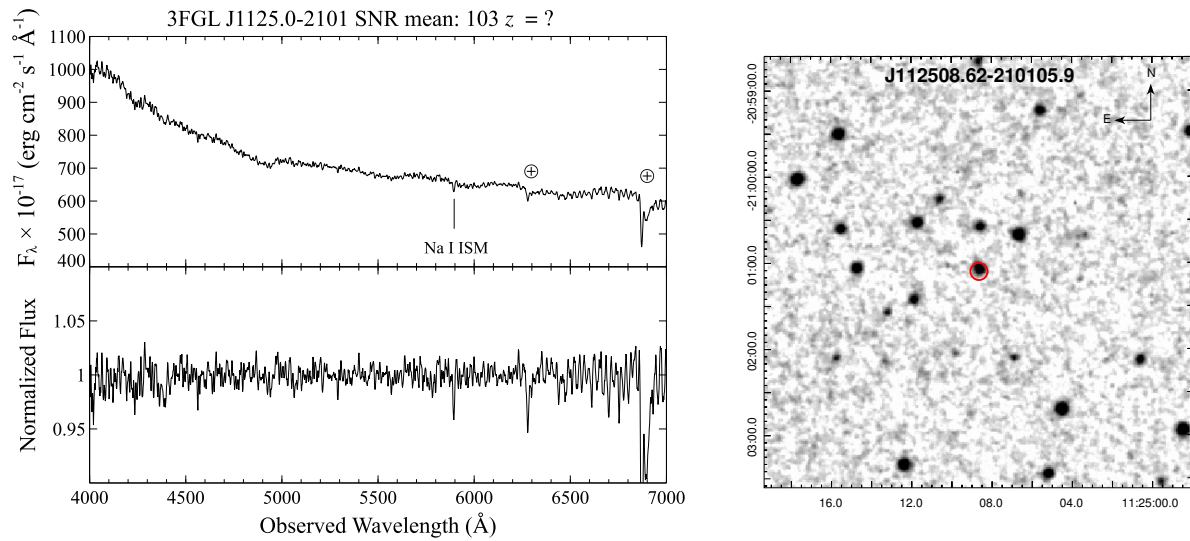


Fig. 30 (Left panel) Optical spectrum of WISE J112508.62-210105.9 associated with 3FGL J1125.0-2101, in the upper part it is shown the Signal-to-Noise Ratio of the spectrum. (Right panel) The finding chart ($5' \times 5'$) retrieved from the Digital Sky Survey highlighting the location of the counterpart: WISE J112508.62-210105.9 (red circle).

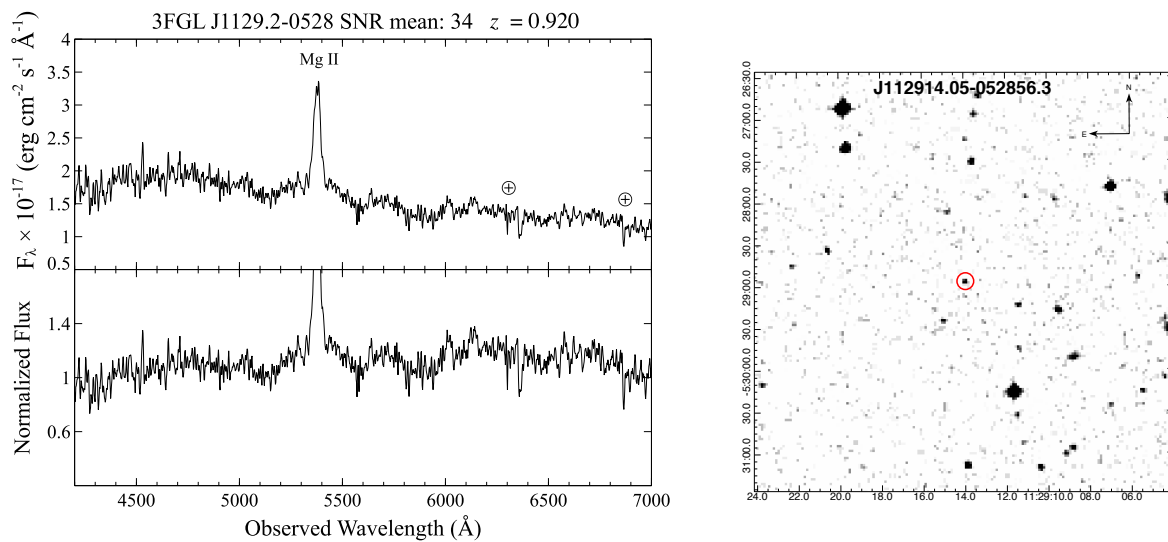


Fig. 31 (Left panel) Optical spectrum of WISE J112914.05-052856.3 associated with 3FGL J1129.2-0528. Signal-to-noise ratio is reported in the Figure. (Right panel) The finding chart ($5' \times 5'$) retrieved from the Digital Sky Survey highlighting the location of the potential source: WISE J112914.05-052856.3 (red circle).

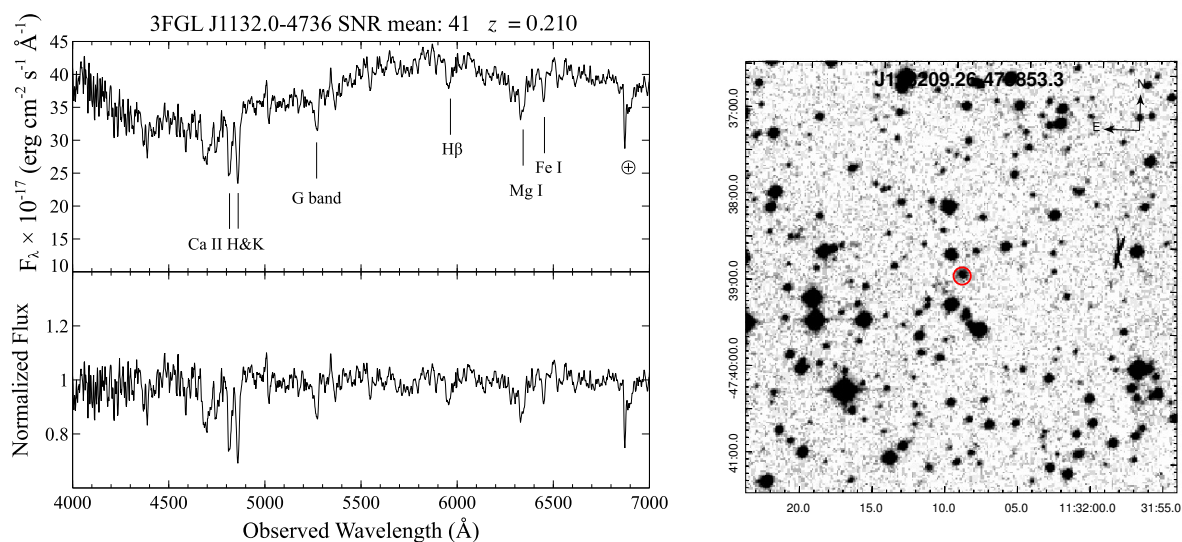


Fig. 32 (Left panel) Optical spectrum of WISE J113209.26-473853.3 associated with 3FGL J1132.0-4736. Signal-to-noise ratio is reported in the Figure. (Right panel) The finding chart ($5' \times 5'$) retrieved from the Digital Sky Survey highlighting the location of the potential source: WISE J113209.26-473853.3 (red circle).

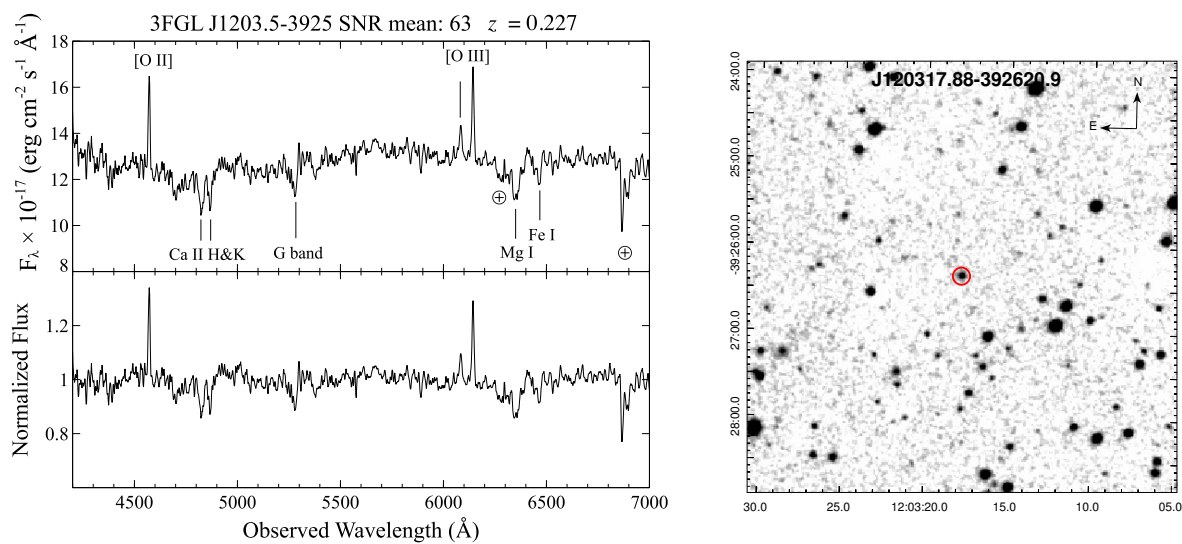


Fig. 33 (Left panel) Optical spectrum of WISE J120317.88-392620.9 associated with 3FGL J1203.5-3925, in the upper part it is shown the Signal-to-Noise Ratio of the spectrum. (Right panel) The finding chart ($5' \times 5'$) retrieved from the Digital Sky Survey highlighting the location of the counterpart: WISE J120317.88-392620.9 (red circle).

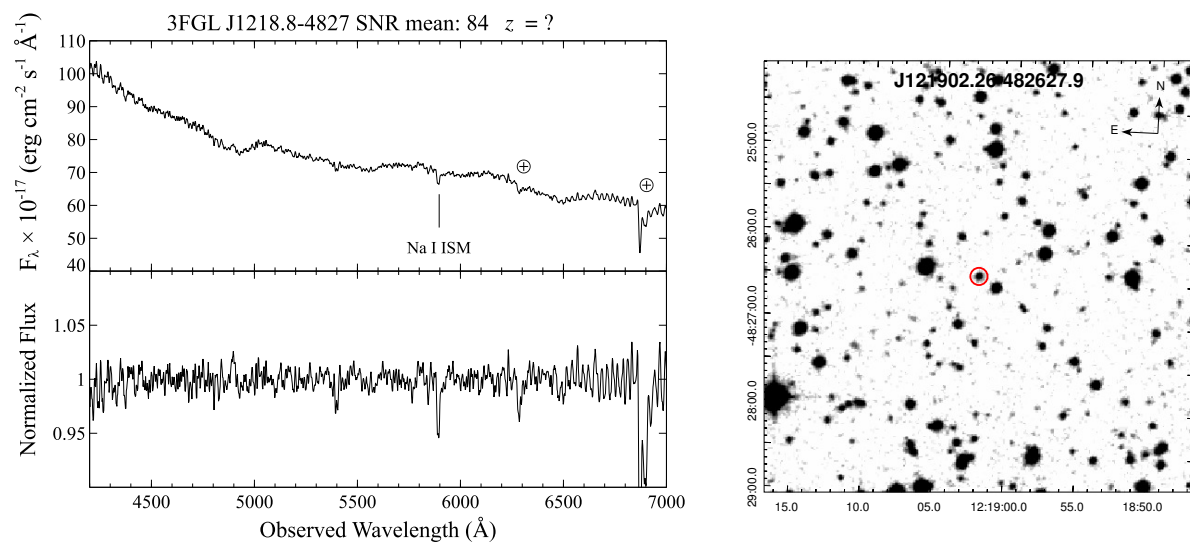


Fig. 34 (Left panel) Optical spectrum of WISE J121902.26-482627.9 associated with 3FGL J1218.8-4827, in the upper part it is shown the Signal-to-Noise Ratio of the spectrum. (Right panel) The finding chart ($5' \times 5'$) retrieved from the Digital Sky Survey highlighting the location of the counterpart: WISE J121902.26-482627.9 (red circle).

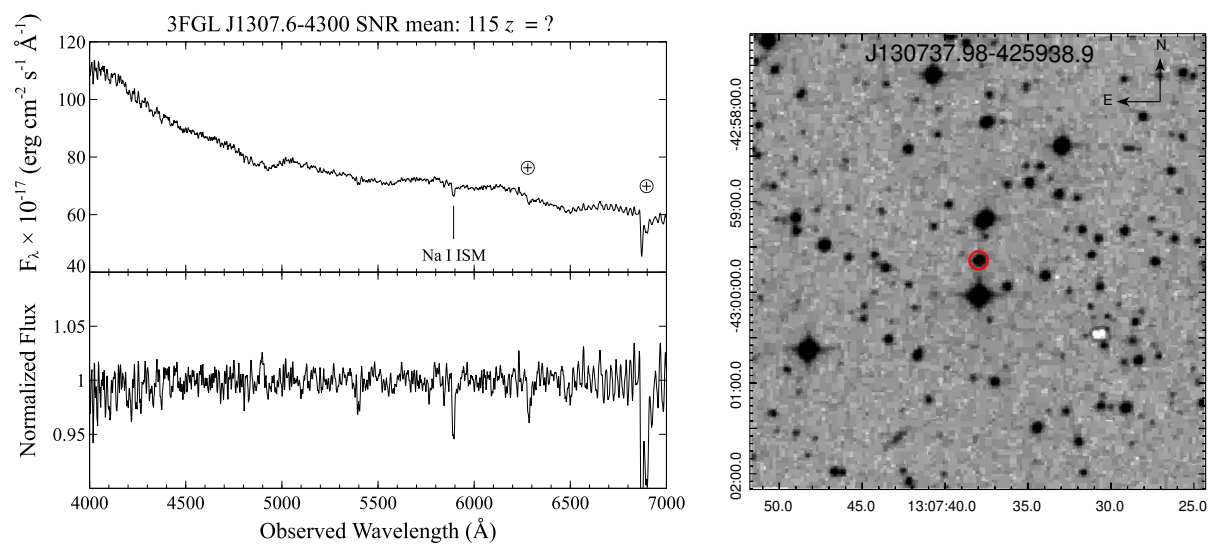


Fig. 35 (Left panel) Optical spectrum of WISE J130737.98-425938.9 associated with 3FGL J1307.6-4300, in the upper part it is shown the Signal-to-Noise Ratio of the spectrum. (Right panel) The finding chart ($5' \times 5'$) retrieved from the Digital Sky Survey highlighting the location of the counterpart: WISE J130737.98-425938.9 (red circle).

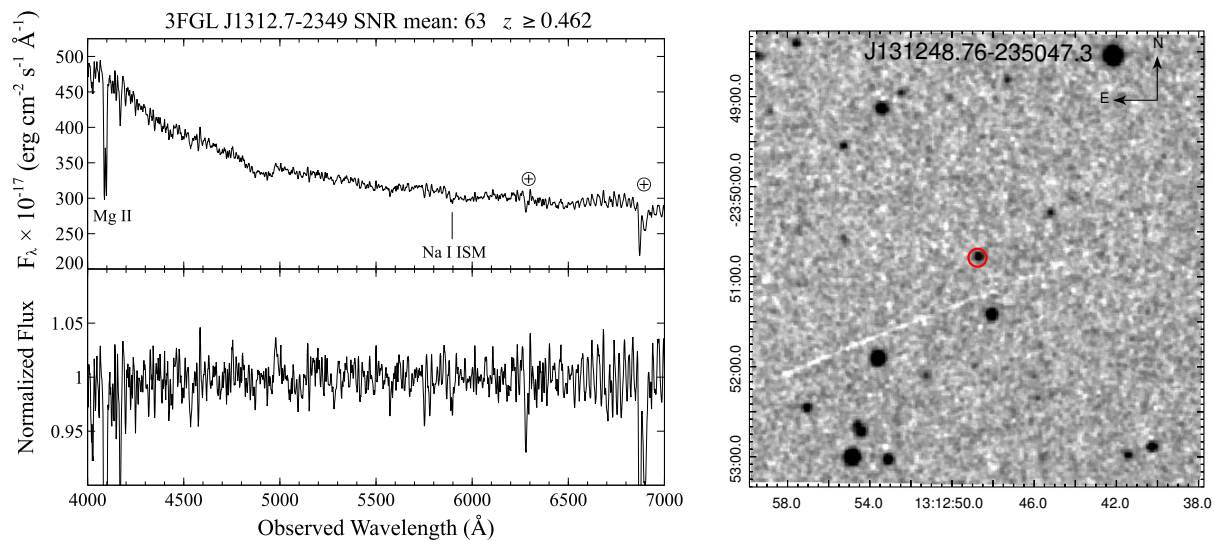


Fig. 36 (Left panel) Optical spectrum of WISE J131248.76-235047.3 associated with 3FGL J1312.7-2349, in the upper part it is shown the Signal-to-Noise Ratio of the spectrum. (Right panel) The finding chart ($5' \times 5'$) retrieved from the Digital Sky Survey highlighting the location of the counterpart: WISE J131248.76-235047.3 (red circle).

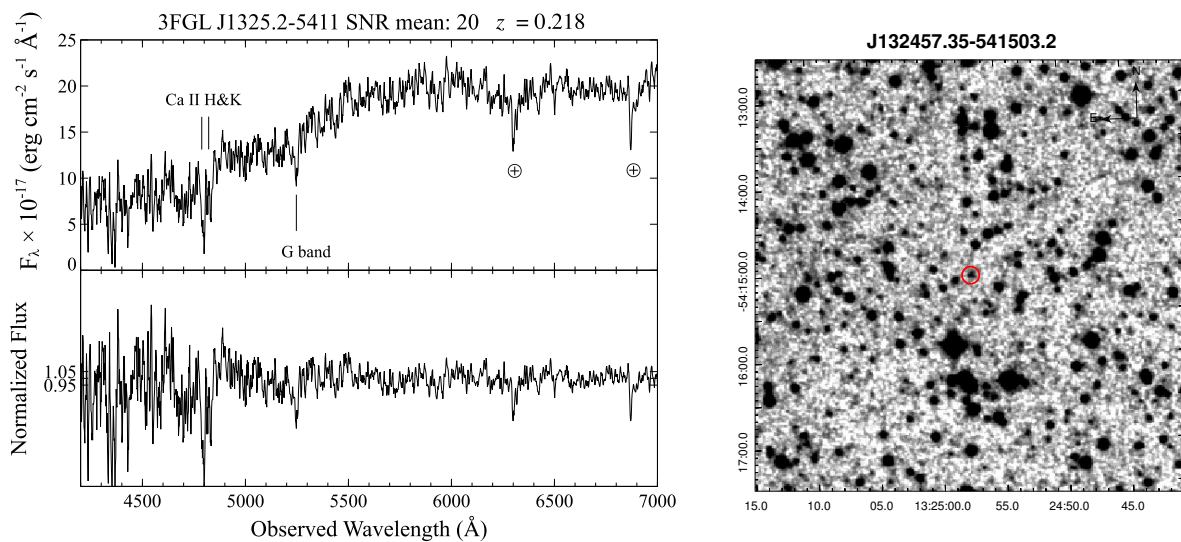


Fig. 37 (Left panel) Optical spectrum of WISE J132457.35-541503.2 associated with 3FGL J1325.2-5411. Signal-to-noise ratio is reported in the Figure. (Right panel) The finding chart ($5' \times 5'$) retrieved from the Digital Sky Survey highlighting the location of the potential source: WISE J132457.35-541503.2 (red circle).

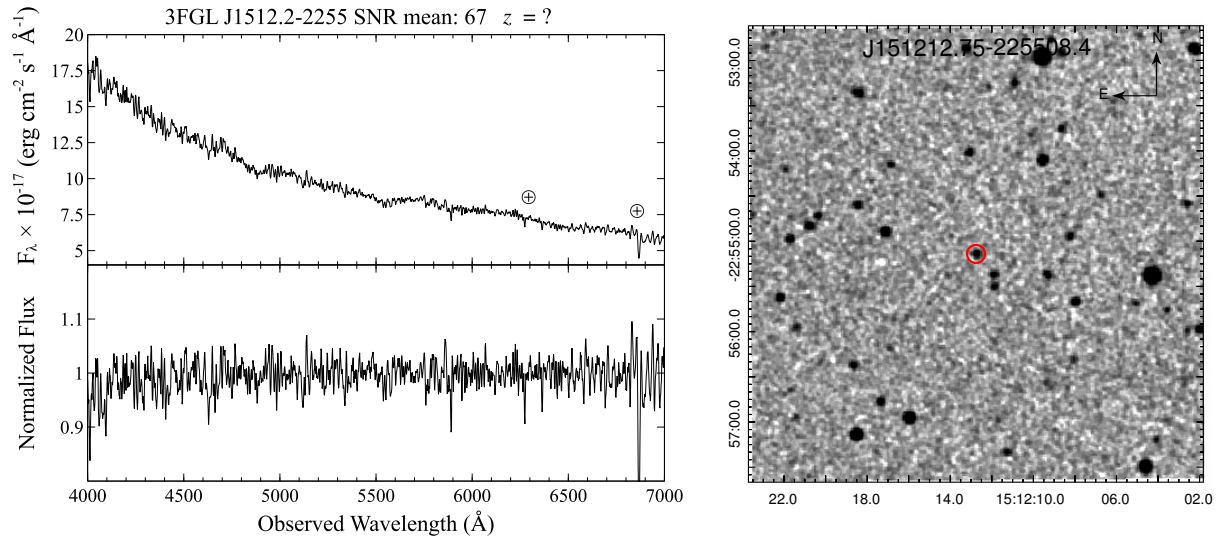


Fig. 38 (Left panel) Optical spectrum of WISE J151212.75-225508.4 associated with 3FGL J1512.2-2255, in the upper part it is shown the Signal-to-Noise Ratio of the spectrum. (Right panel) The finding chart ($5' \times 5'$) retrieved from the Digital Sky Survey highlighting the location of the counterpart: WISE J151212.75-225508.4 (red circle).

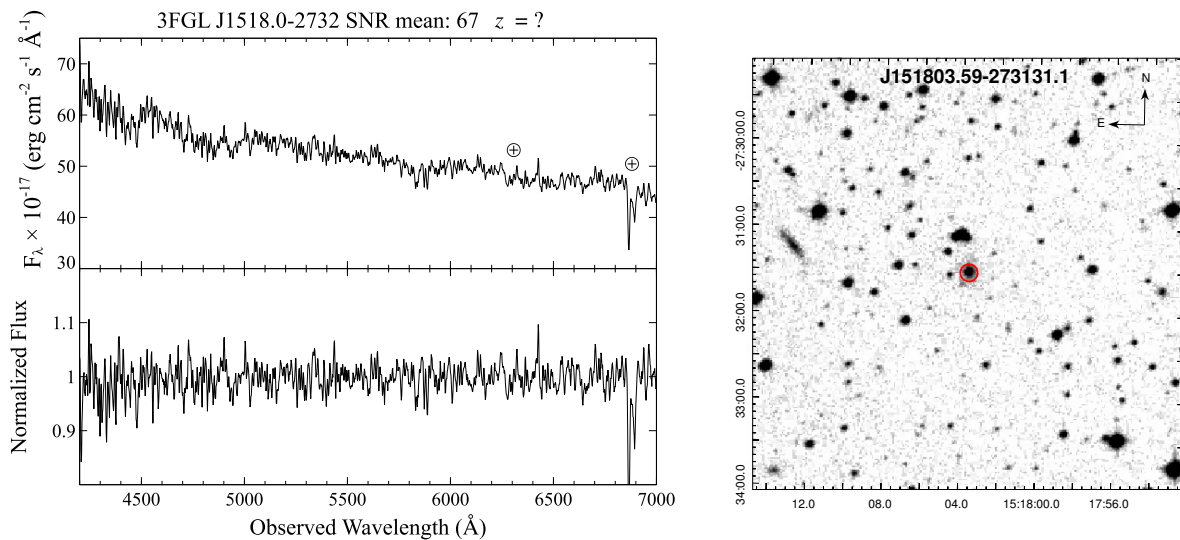


Fig. 39 (Left panel) Optical spectrum of WISE J151803.59-273131.1 associated with 3FGL J1518.0-2732, in the upper part it is shown the Signal-to-Noise Ratio of the spectrum. (Right panel) The finding chart ($5' \times 5'$) retrieved from the Digital Sky Survey highlighting the location of the counterpart: WISE J151803.59-273131.1 (red circle).

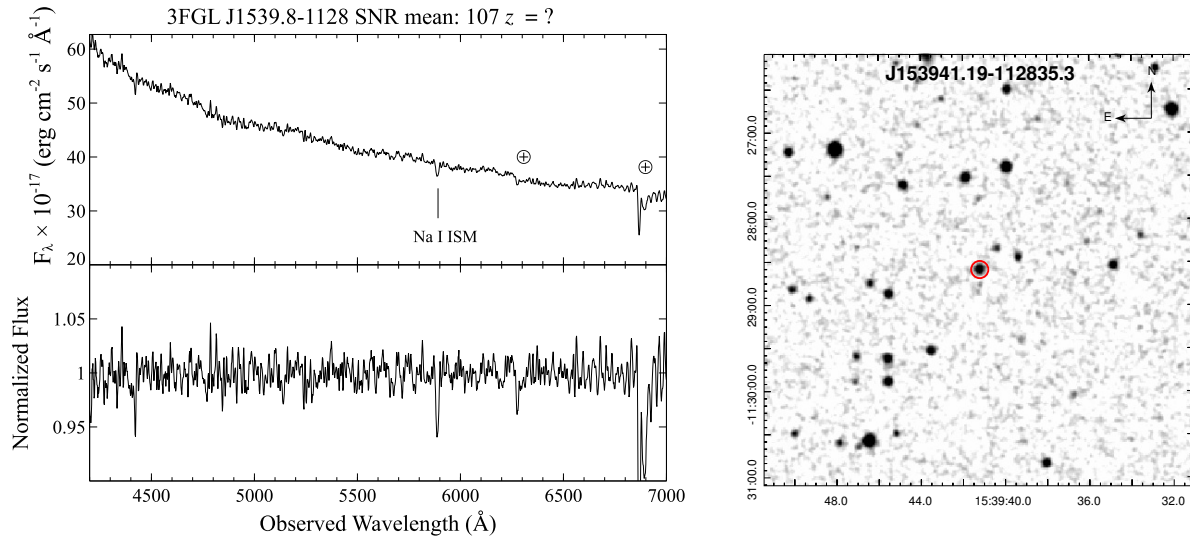


Fig. 40 (Left panel) Optical spectrum of WISE J153941.19-112835.3 associated with 3FGL J1539.8-1128, in the upper part it is shown the Signal-to-Noise Ratio of the spectrum. (Right panel) The finding chart ($5' \times 5'$) retrieved from the Digital Sky Survey highlighting the location of the counterpart: WISE J153941.19-112835.3 (red circle).

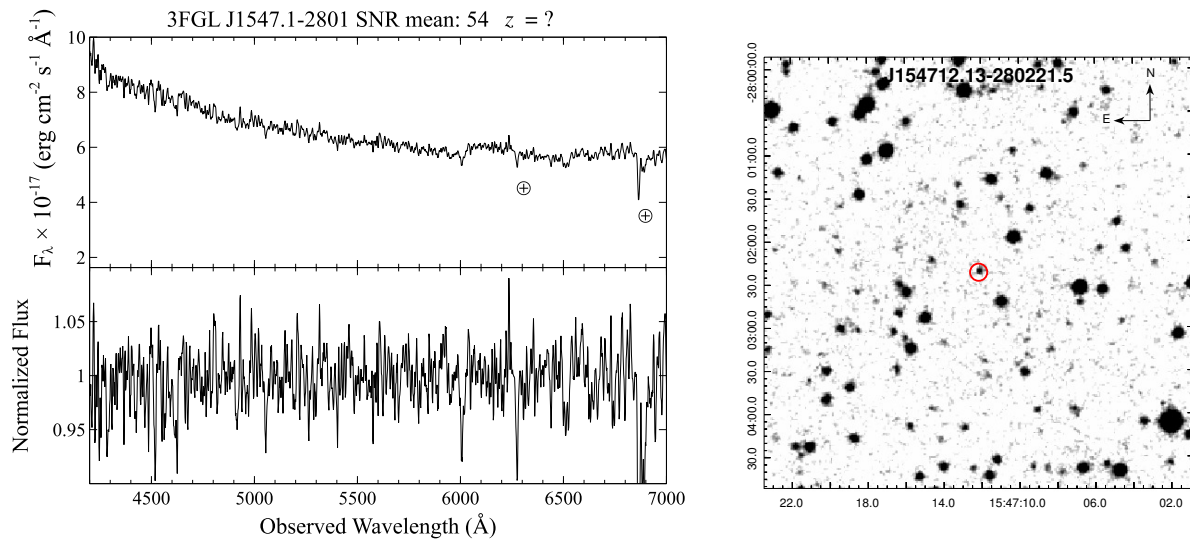


Fig. 41 (Left panel) Optical spectrum of WISE J154712.13-280221.5 associated with 3FGL J1547.1-2801, in the upper part it is shown the Signal-to-Noise Ratio of the spectrum. (Right panel) The finding chart ($5' \times 5'$) retrieved from the Digital Sky Survey highlighting the location of the counterpart: WISE J154712.13-280221.5 (red circle).

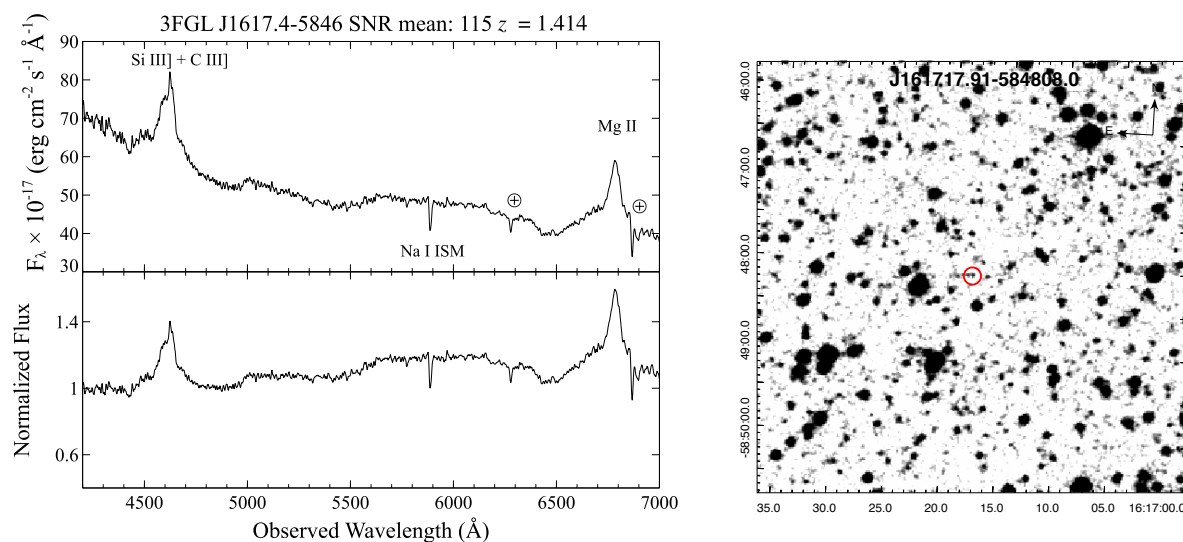


Fig. 42 (Left panel) Optical spectrum of WISE J161717.91-584808.0 associated with 3FGL J1617.4-5846. Signal-to-noise ratio is reported in the Figure. (Right panel) The finding chart ($5' \times 5'$) retrieved from the Digital Sky Survey highlighting the location of the counterpart: WISE J161717.91-584808.0 (red circle).

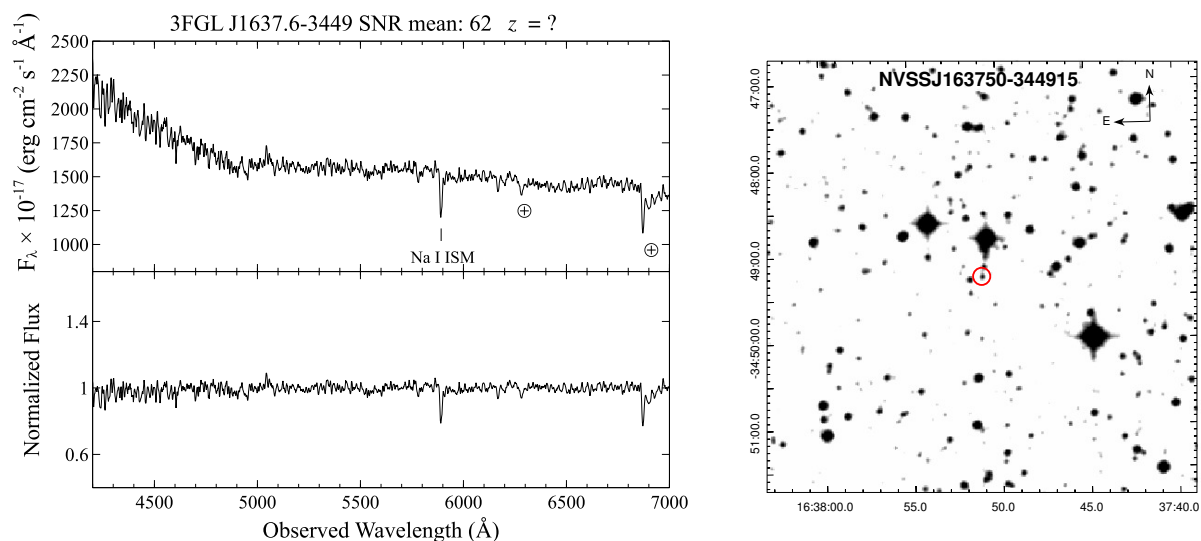


Fig. 43 (Left panel) Optical spectrum of NVSS J163750-344915 associated with 3FGL J1637.6-3449, in the upper part it is shown the Signal-to-Noise Ratio of the spectrum. (Right panel) The finding chart ($5' \times 5'$) retrieved from the Digital Sky Survey highlighting the location of the counterpart: NVSS J163750-344915 (red circle).

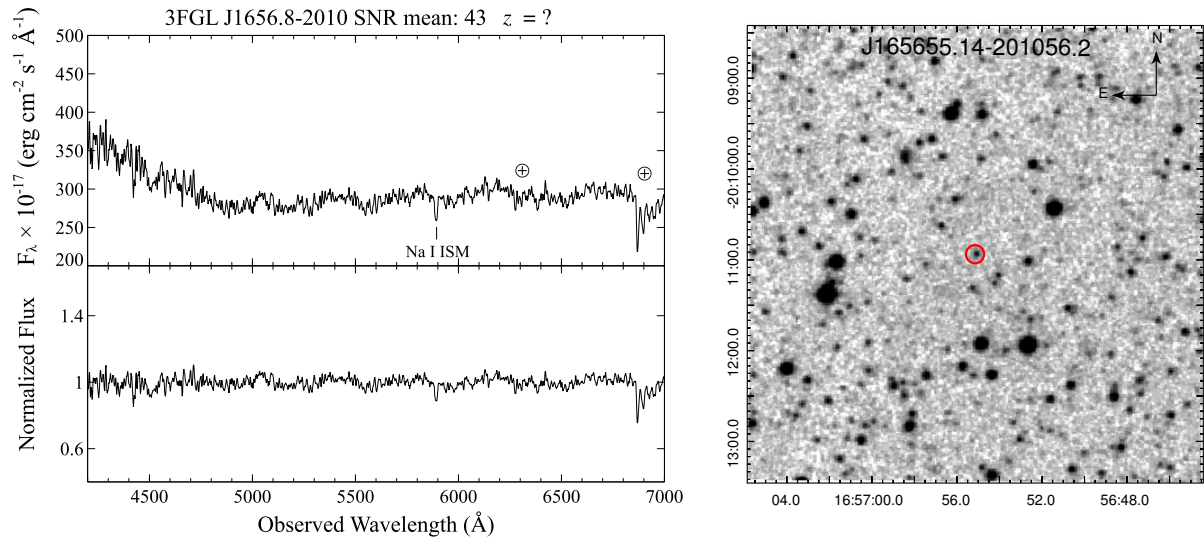


Fig. 44 (Left panel) Optical spectrum of WISE J165655.14-201056.2 associated with 3FGL J1656.8-2010, in the upper part it is shown the Signal-to-Noise Ratio of the spectrum. (Right panel) The finding chart ($5' \times 5'$) retrieved from the Digital Sky Survey highlighting the location of the counterpart: WISE J165655.14-201056.2 (red circle).

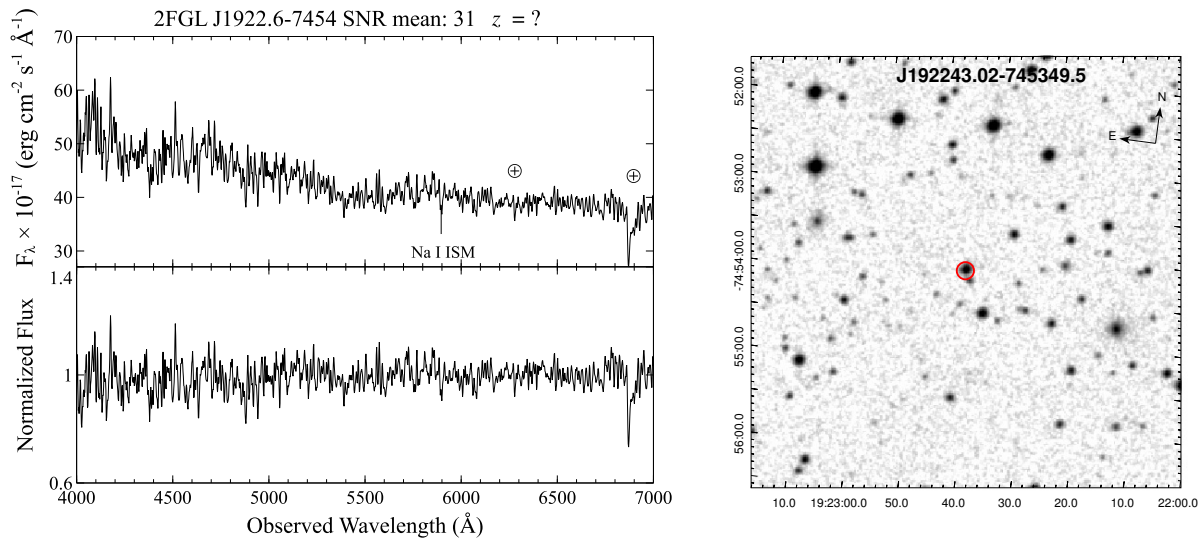


Fig. 45 (Left panel) Optical spectrum of WISE J192243.02-745349.5 associated with 2FGL J1922.6-7454, in the upper part it is shown the Signal-to-Noise Ratio of the spectrum. (Right panel) The finding chart ($5' \times 5'$) retrieved from the Digital Sky Survey highlighting the location of the counterpart: WISE J192243.02-745349.5 (red circle).

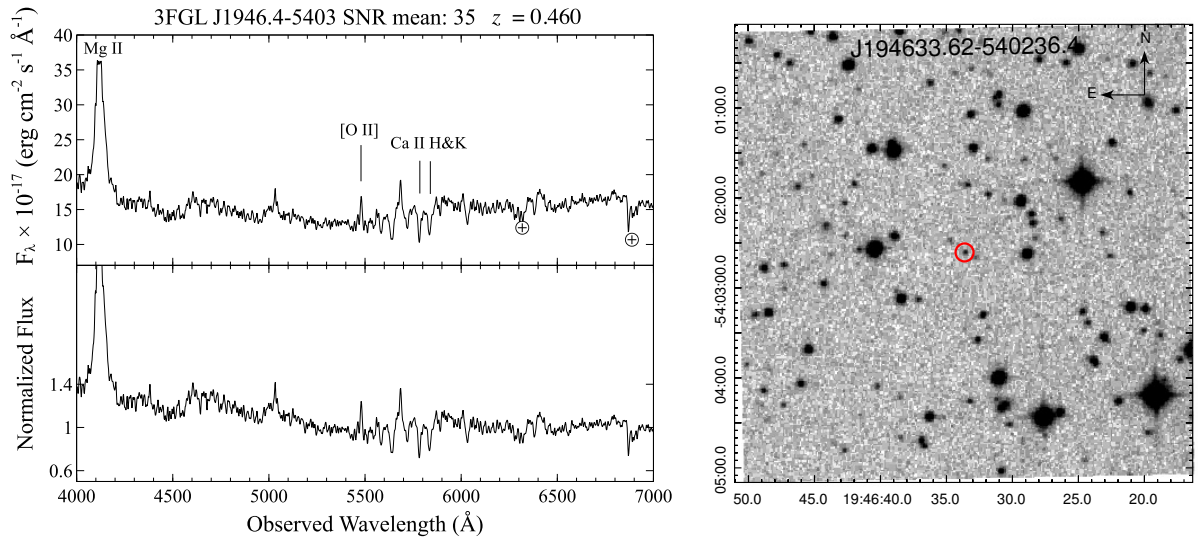


Fig. 46 (Left panel) Optical spectrum of WISE J194633.62-540236.4 associated with 3FGL J1946.4-5403. Signal-to-noise ratio is reported in the Figure. (Right panel) The finding chart ($5' \times 5'$) retrieved from the Digital Sky Survey highlighting the location of the potential source: WISE J194633.62-540236.4 (red circle).

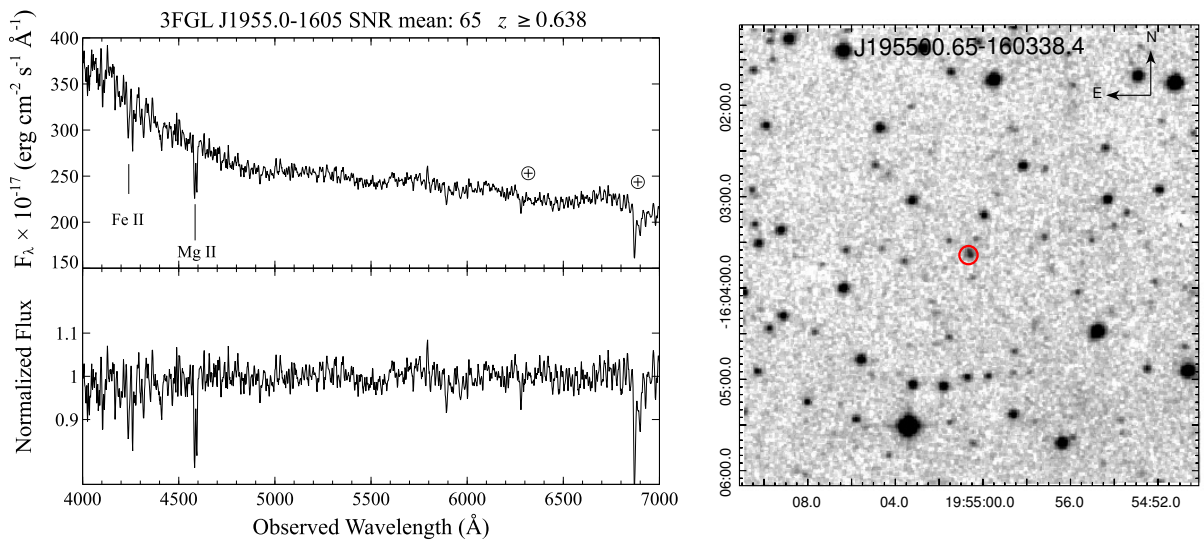


Fig. 47 (Left panel) Optical spectrum of WISE J195500.65-160338.4 associated with 3FGL J1955.0-1605, in the upper part it is shown the Signal-to-Noise Ratio of the spectrum. (Right panel) The finding chart ($5' \times 5'$) retrieved from the Digital Sky Survey highlighting the location of the counterpart: WISE J195500.65-160338.4 (red circle).

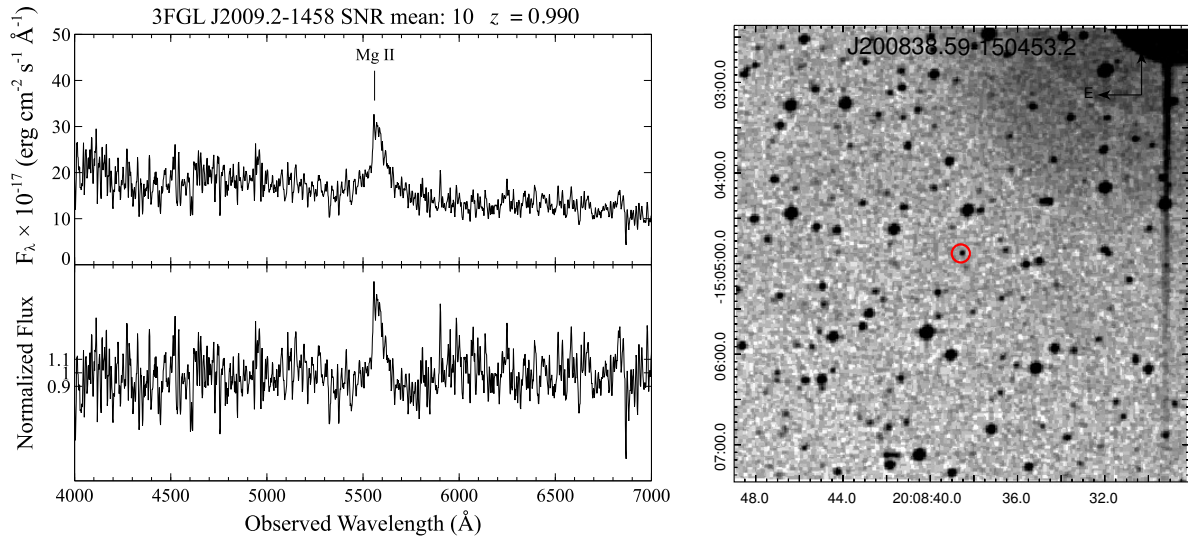


Fig. 48 (Left panel) Optical spectrum of WISE J200838.59-150453.2 associated with 3FGL J2009.2-1458. Signal-to-noise ratio is reported in the Figure. (Right panel) The finding chart (5' × 5') retrieved from the Digital Sky Survey highlighting the location of the potential source: WISE J200838.59-150453.2 (red circle).

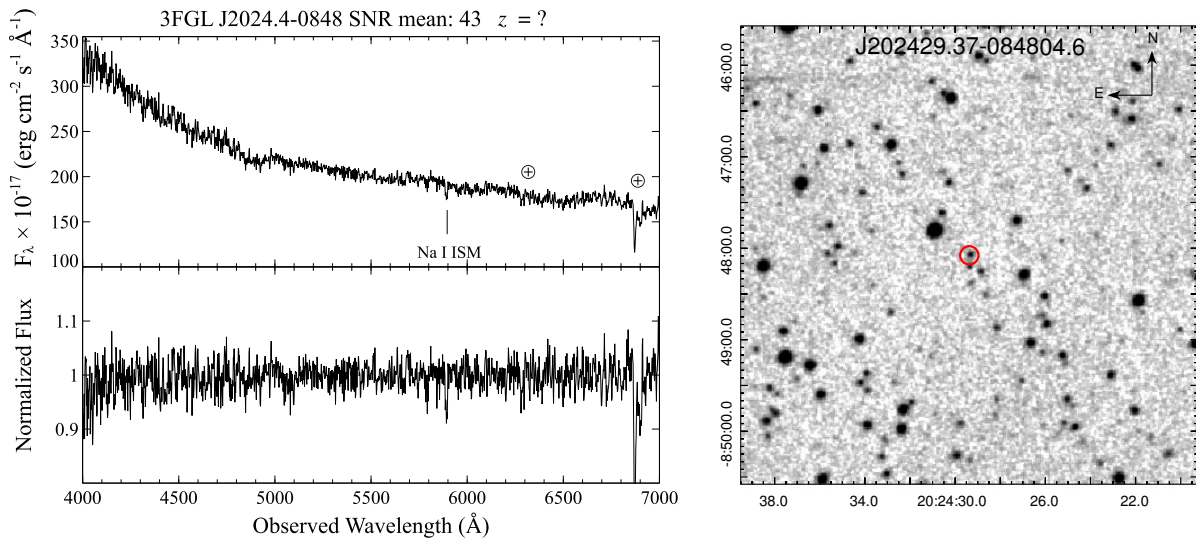


Fig. 49 (Left panel) Optical spectrum of WISE J202429.37-084804.6 associated with 3FGL J2024.4-0848. Signal-to-noise ratio is reported in the Figure. (Right panel) The finding chart (5' × 5') retrieved from the Digital Sky Survey highlighting the location of the counterpart: WISE J202429.37-084804.6 (red circle).

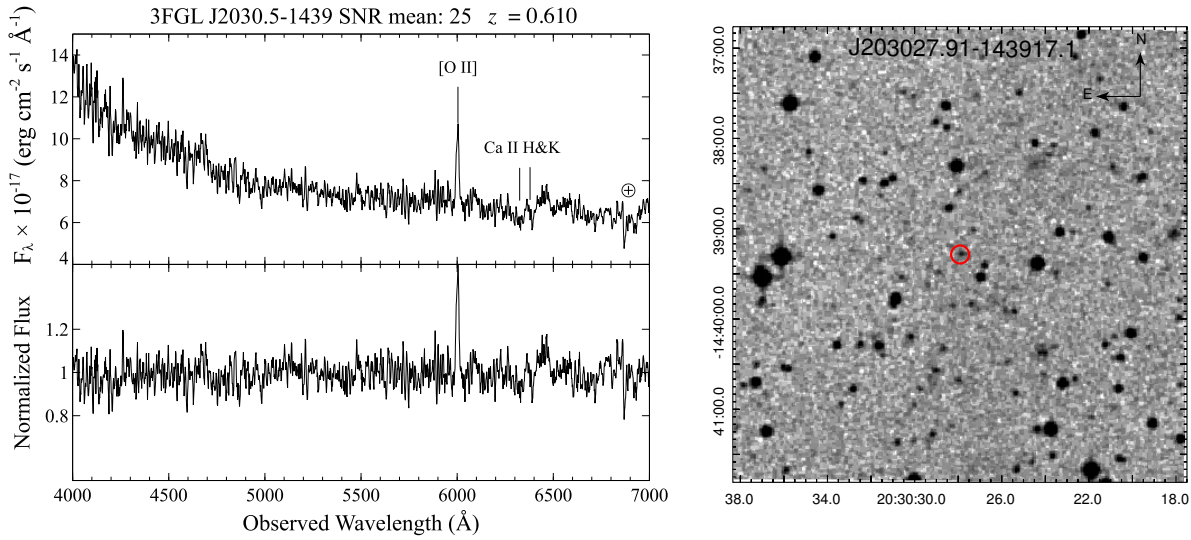


Fig. 50 (Left panel) Optical spectrum of WISE J203027.91-143917.1 associated with 3FGL J2030.5-1439. Signal-to-noise ratio is reported in the Figure. (Right panel) The finding chart ($5' \times 5'$) retrieved from the Digital Sky Survey highlighting the location of the potential source: WISE J203027.91-143917.1 (red circle).

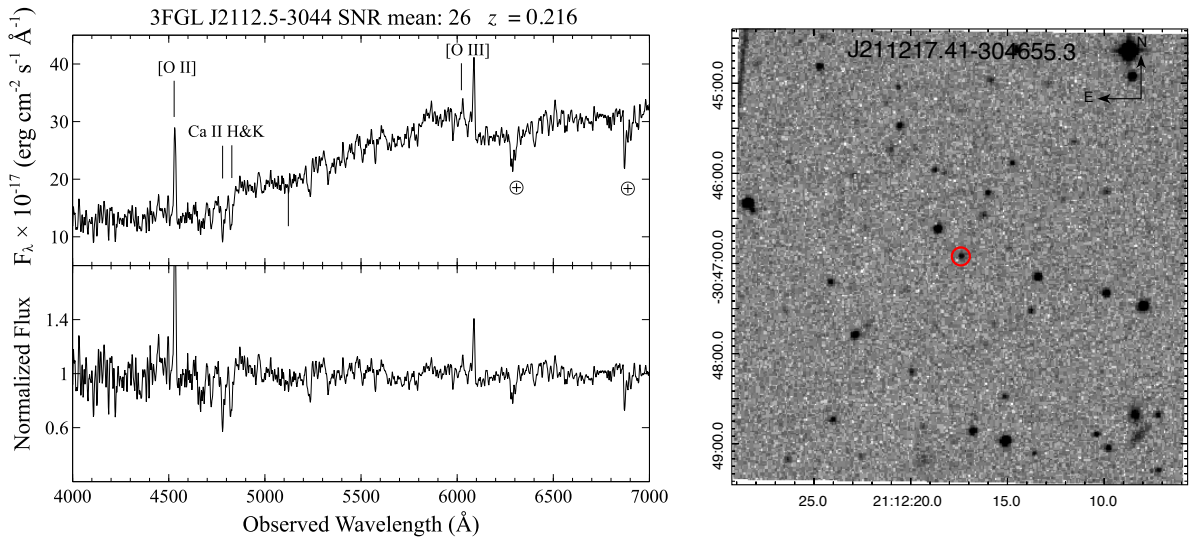


Fig. 51 (Left panel) Optical spectrum of WISE J211217.41-304655.3 associated with 3FGL J2112.5-3044. Signal-to-noise ratio is reported in the Figure. (Right panel) The finding chart ($5' \times 5'$) retrieved from the Digital Sky Survey highlighting the location of the potential source: WISE J211217.41-304655.3 (red circle).

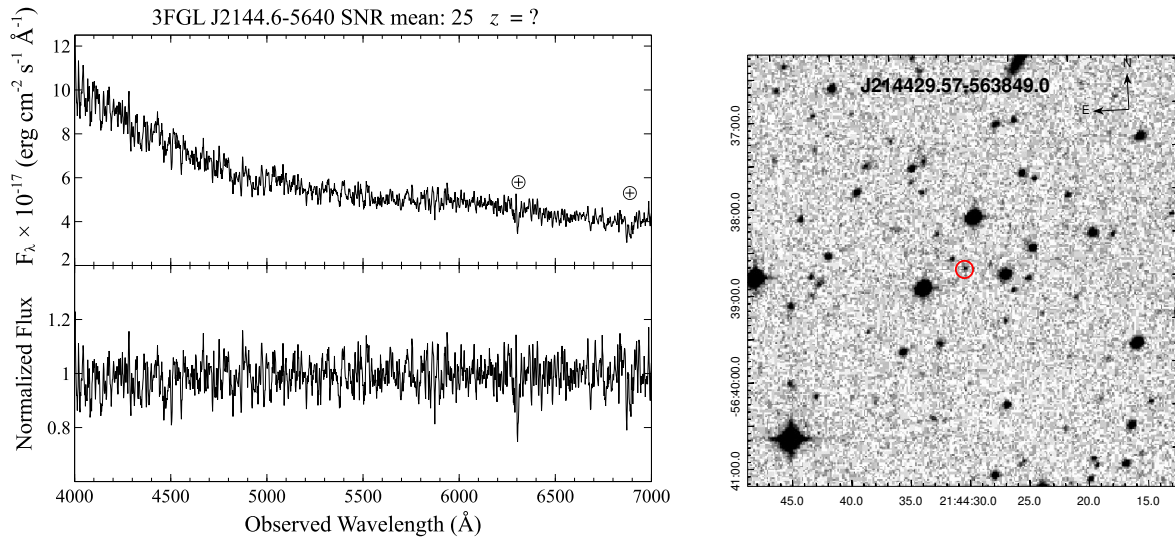


Fig. 52 (Left panel) Optical spectrum of WISE J214429.57-563849.0 associated with 3FGL J2144.6-5640. Signal-to-noise ratio is reported in the Figure. (Right panel) The finding chart (5' x 5') retrieved from the Digital Sky Survey highlighting the location of the potential source: WISE J214429.57-563849.0 (red circle).

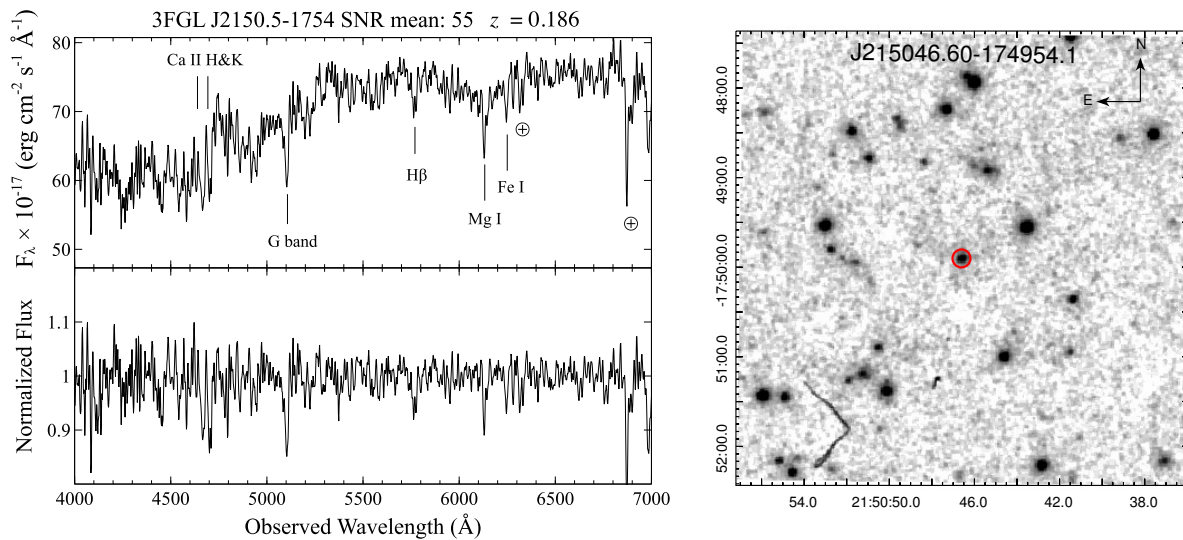


Fig. 53 (Left panel) Optical spectrum of WISE J215046.60-174954.1 associated with 3FGL J2150.5-1754. Signal-to-noise ratio is reported in the Figure. (Right panel) The finding chart (5' x 5') retrieved from the Digital Sky Survey highlighting the location of the potential source: WISE J215046.60-174954.1 (red circle).

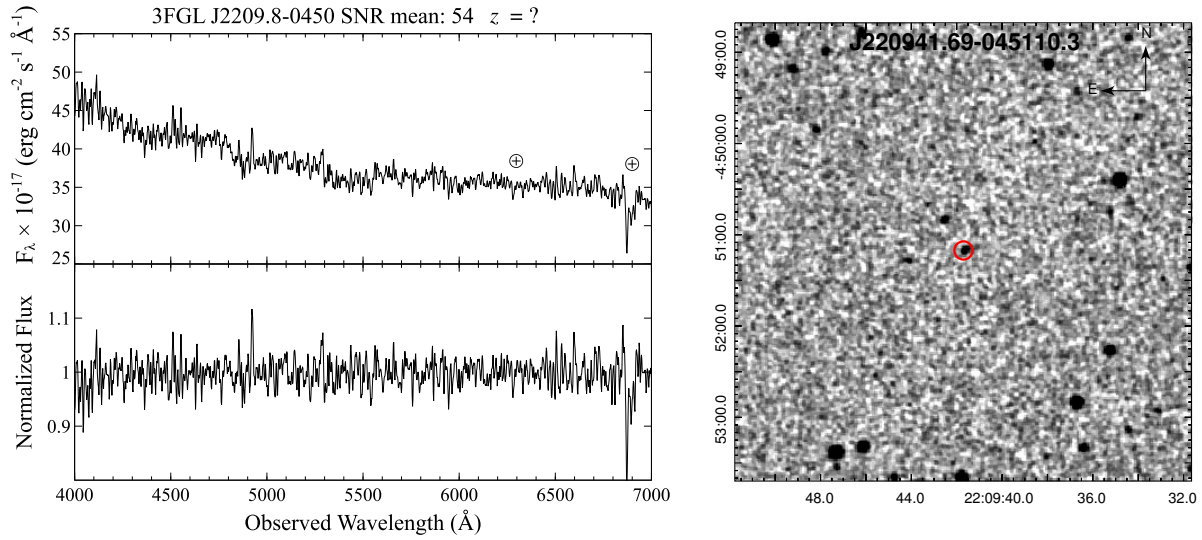


Fig. 54 (Left panel) Optical spectrum of WISE J220941.69-045110.3 associated with 3FGL J2209.8-0450. Signal-to-noise ratio is reported in the Figure. (Right panel) The finding chart ($5' \times 5'$) retrieved from the Digital Sky Survey highlighting the location of the potential source: WISE J220941.69-045110.3 (red circle).

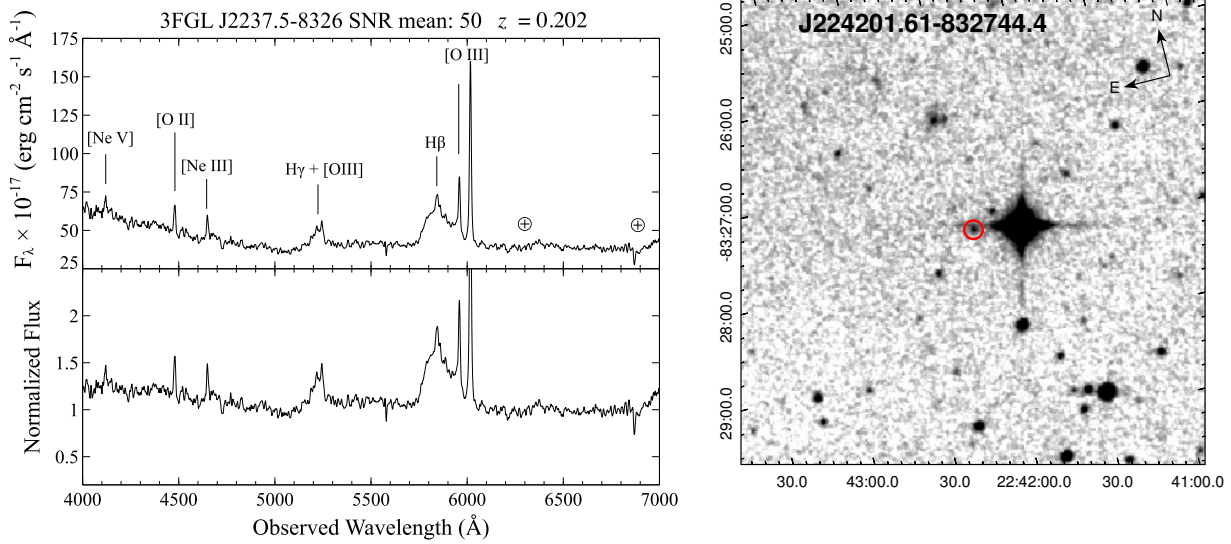


Fig. 55 (Left panel) Optical spectrum of WISE J224201.61-832744.4 associated with 3FGL J2237.5-8326. Signal-to-noise ratio is reported in the Figure. (Right panel) The finding chart ($5' \times 5'$) retrieved from the Digital Sky Survey highlighting the location of the potential source: WISE J224201.61-832744.4 (red circle).

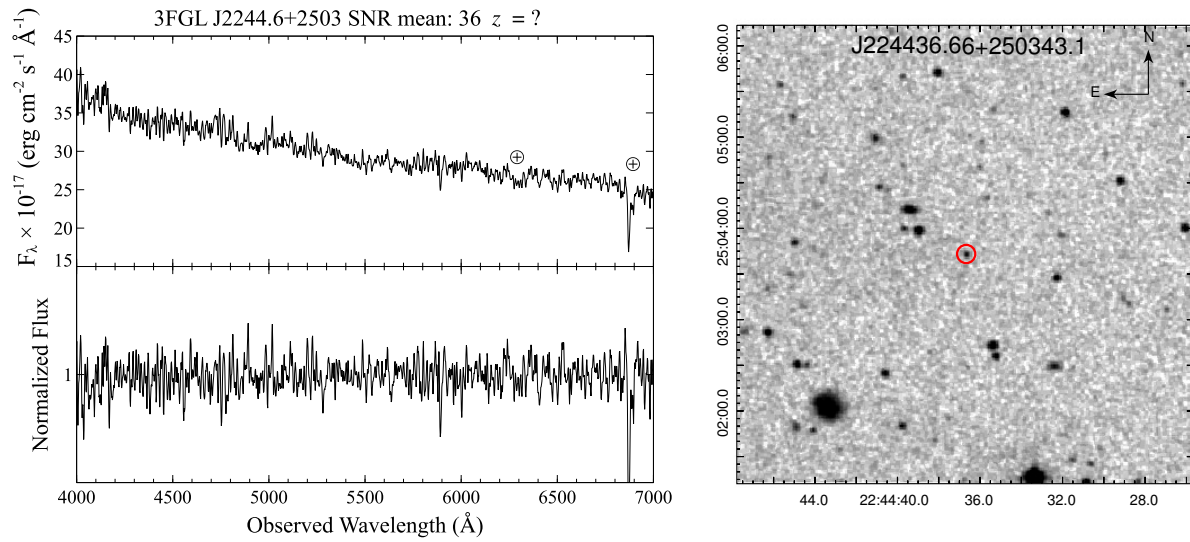


Fig. 56 (Left panel) Optical spectrum of WISE J224436.66+250343.1 associated with 3FGL J2244.6+2503. Signal-to-noise ratio is reported in the Figure. (Right panel) The finding chart ($5' \times 5'$) retrieved from the Digital Sky Survey highlighting the location of the potential source: WISE J224436.66+250343.1 (red circle).

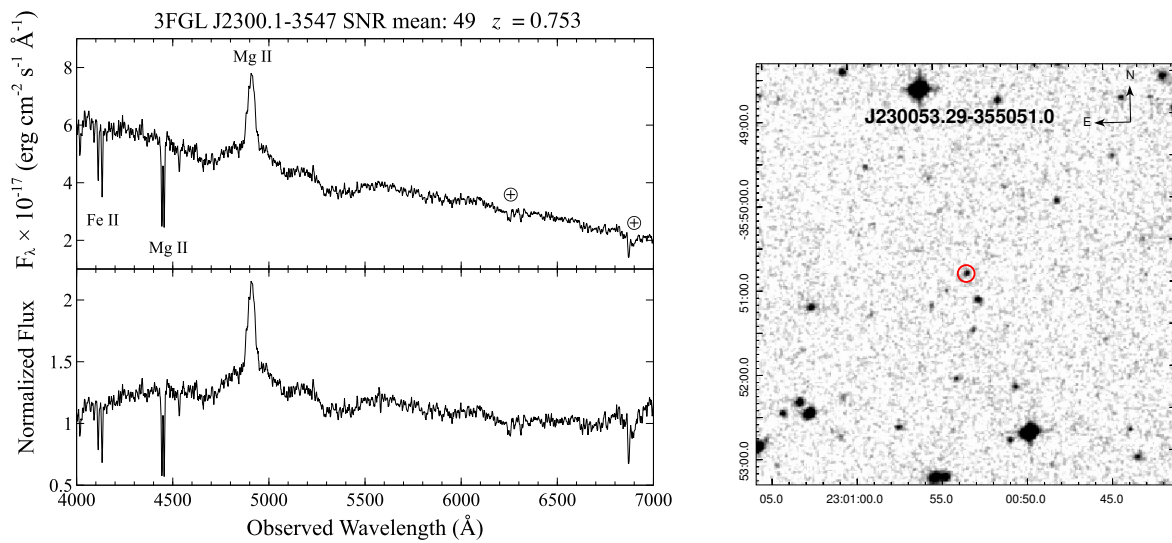


Fig. 57 (Left panel) Optical spectrum of WISE J230053.29-355051.0 associated with 3FGL J2300.1-3547. Signal-to-noise ratio is reported in the Figure. (Right panel) The finding chart ($5' \times 5'$) retrieved from the Digital Sky Survey highlighting the location of the potential source: WISE J230053.29-355051.0 (red circle).

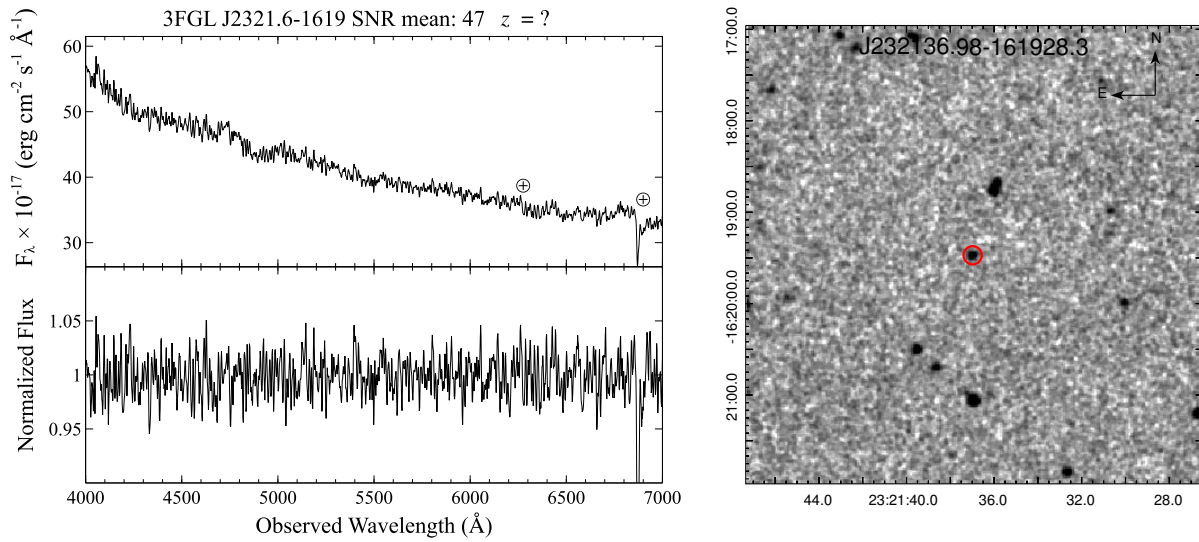


Fig. 58 (Left panel) Optical spectrum of WISE J232136.98-161928.3 associated with 3FGL J2321.6-1619. Signal-to-noise ratio is reported in the Figure. (Right panel) The finding chart ($5' \times 5'$) retrieved from the Digital Sky Survey highlighting the location of the potential source: WISE J232136.98-161928.3 (red circle).

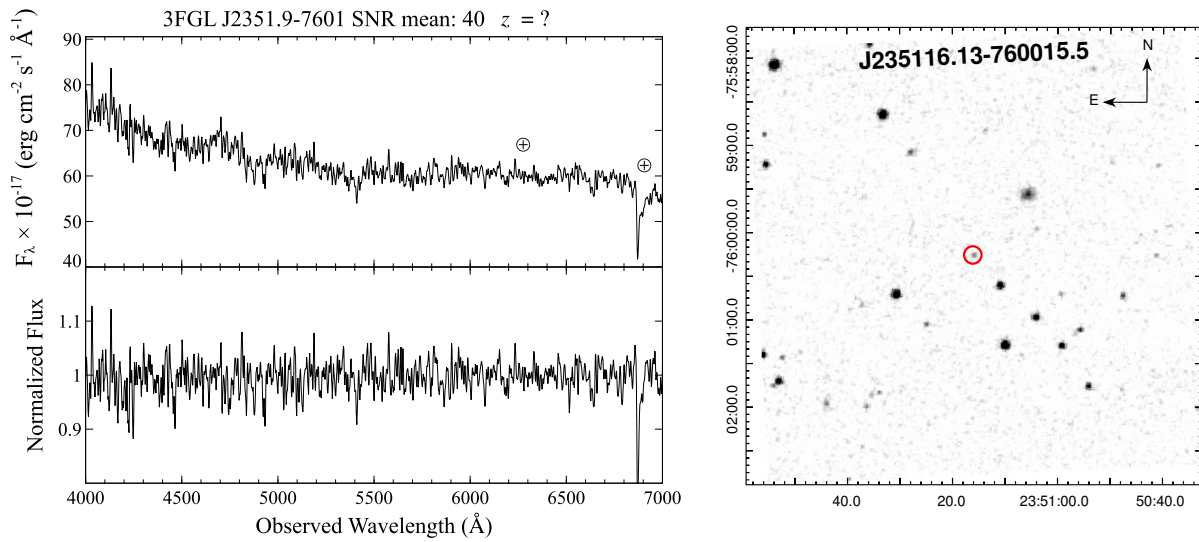


Fig. 59 (Left panel) Optical spectrum of WISE J235116.13-760015.5 associated with 3FGL J2351.9-7601. Signal-to-noise ratio is reported in the Figure. (Right panel) The finding chart ($5' \times 5'$) retrieved from the Digital Sky Survey highlighting the location of the potential source: WISE J235116.13-760015.5 (red circle).

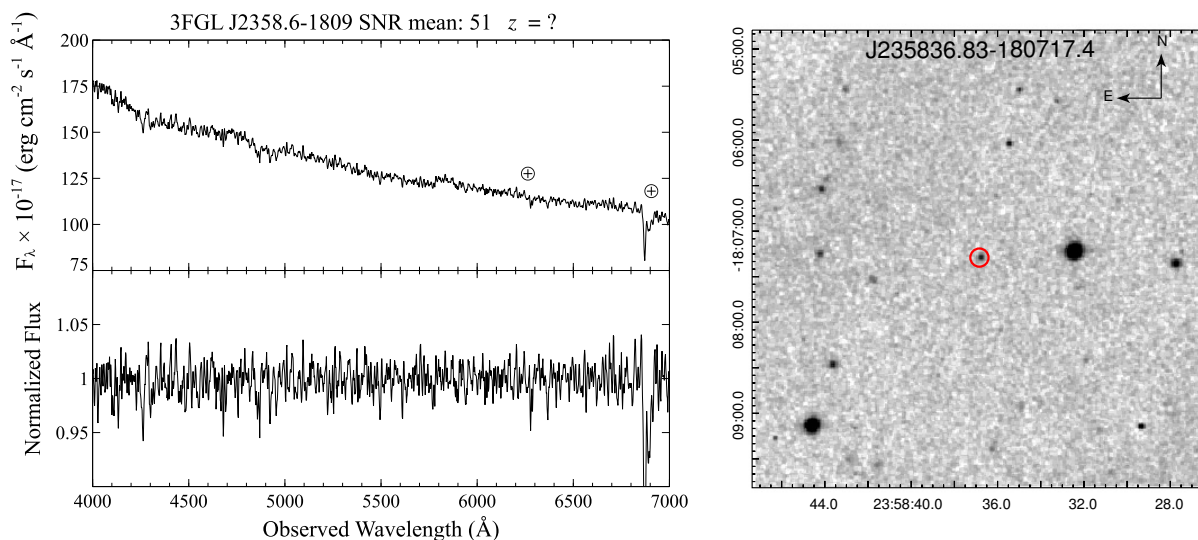


Fig. 60 (Left panel) Optical spectrum of WISE J235836.83-180717.4 associated with 3FGL J2358.6-1809. Signal-to-noise ratio is reported in the Figure. (Right panel) The finding chart ($5' \times 5'$) retrieved from the Digital Sky Survey highlighting the location of the potential source: WISE J235836.83-180717.4 (red circle).

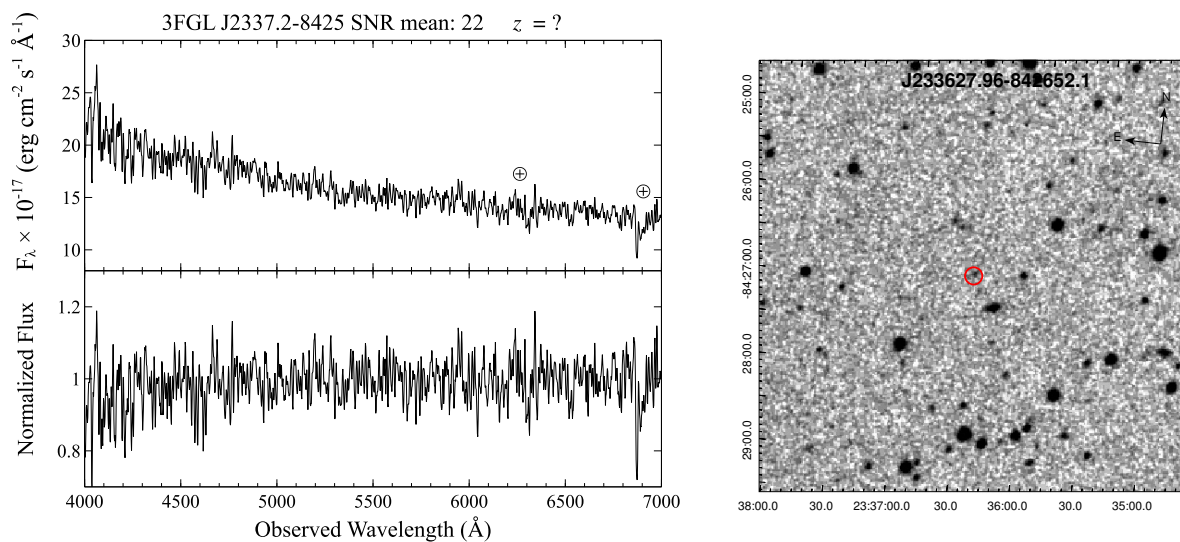


Fig. 61 (Left panel) Optical spectrum of WISE J233627.96-842652.1 associated with 3FGL J2337.2-8425. Signal-to-noise ratio is reported in the Figure. (Right panel) The finding chart ($5' \times 5'$) retrieved from the Digital Sky Survey highlighting the location of the potential source: WISE J233627.96-842652.1 (red circle).

We acknowledge Dr. S. Points for the support while carrying out the SOAR observations. Work by C.C.C. at NRL is supported in part by NASA DPR S-15633-Y. H. A. Smith acknowledges partial support from NASA grants NNX14AJ61G and NNX15AE56G JS acknowledges support from NASA grant NNX15AU83G and a Packard Fellowship. EJB acknowledges support from Programa de Apoyo a Proyectos de Investigación e Innovación Tecnológica (IN109217). This publication makes use of data products from the Wide-field Infrared Survey Explorer, which is a joint project of the University of California, Los Angeles, and the Jet Propulsion Laboratory/California Institute of Technology, funded by the National Aeronautics and Space Administration. Based on observations obtained at the Southern Astrophysical Research (SOAR) telescope, which is a joint project of the Ministério da Ciência, Tecnologia, e Inovação (MCTI) da República Federativa do Brasil, the U.S. National Optical Astronomy Observatory (NOAO), the University of North Carolina at Chapel Hill (UNC), and Michigan State University (MSU). TOPCAT¹ (Taylor 2005) for the preparation and manipulation of the tabular data.

¹<http://www.star.bris.ac.uk/~mbt/topcat/>

References

- Abdo, A. A., Ackermann, M., Ajello, M. et al. 2010a ApJS, 188, 405
- Abdo, A. A., Ackermann, M., Agudo, I., Ajello, M. et al. 2010b ApJ 716
- Acero, F., Donato, D., Ojha, R. et al. 2013 ApJ, 779, 133
- Acero, F., Ackermann, M., Ajello, M., et al. 2015 ApJS, 218, 23
- Ackermann, M., Ajello, M., Atwood, W. B. et al. 2015 ApJ, 810, 14
- Ahn, C. P., Alexandroff, R., Allende Prieto, C., et al. 2012, ApJS, 203, 21
- Álvarez Crespo, N., Masetti, N., Landoni, M. et al. 2016 AJ, 151, 32
- Álvarez Crespo, N., Massaro, F., Milisavljevic, D. et al. 2016 AJ, 151, 95
- Álvarez Crespo, N., Massaro, F., D’Abrusco, R. et al. 2016c ApSS 361, 316
- Atwood, W. B., Abdo, A. A., Ackermann, M. et al. 2009 ApJ, 697, 1071
- Blandford, R. D., & Rees, M. J. 1978, Proc. Pittsburgh Conference on BL Lac objects, 328
- Becker, R. H., White, R. L., Helfand, D. J. 1995 ApJ, 450, 559
- Cardelli, J. A., Clayton, G. C., & Mathis, J. S. 1989, ApJ, 345, 245
- Clemens, J. C., Crain, J. A., & Anderson, R. 2004, Proc. SPIE, 5492, 331
- Condon, J. J., Cotton, W. D., Greisen, E. W., et al. 1998, AJ, 115, 1693
- Cohen, A. S., Lane, W. M., Cotton, W. D., et al. 2007, AJ, 134, 1245.
- Cowperthwaite, P. S., Massaro, F., D’Abrusco, R. et al. 2013 AJ, 146, 110
- D’Abrusco, R., Massaro, F., Ajello, M. et al. 2012 ApJ, 748, 68
- D’Abrusco, R., Massaro, F., Paggi, A. et al. 2013 ApJS, 206, 12
- D’Abrusco, R., Massaro, F., Paggi, A. et al. 2014 ApJS, 215, 14
- Douglas, J. N., Bash, F. N., Bozayan, F. A., Torrence, G. W., & Wolfe, C. 1996, AJ, 111, 1945
- Evans, P. A., Osborne, J. P., Beardmore, A. P., et al. 2014, ApJS, 210, 8
- Evans, I. N., Primini, F. A., Glotfelty, K. J., et al. 2010, ApJS, 189, 37
- Fichtel, C. E., et al. 1994, ApJS, 94, 551
- Fossati G., Maraschi L., Celotti A., Comastri A., Ghisellini G. 1998 MNRAS 299 433F
- Giommi, P., Ansari, S. G., Micol, A. 1995 A&AS 109 267G
- Gioletti, M., Massaro, F., D’Abrusco, R. et al. 2016 A&A, 588A, 141
- Healey, S. E., Romani, R. W., Taylor, G. B., et al. 2007, ApJS, 171, 61
- Jones, H. D., et al. 2004, MNRAS, 355, 747
- Jones, H. D., et al. 2009, MNRAS, 399, 683
- Landoni, M., Massaro, F. et al. 2015 AJ, 149, 63
- Maselli, A., Massaro, F., D’Abrusco, R. et al. 2015 Ap&SS, 357, 141
- Massaro, E., Giommi, P., Leto, C. et al. 2009 A&A, 495, 691
- Massaro, F., D’Abrusco, R., Ajello, M. et al. 2011 ApJ, 740L, 48
- Massaro, F., D’Abrusco, R., Tosti, G. et al. 2012 ApJ, 752, 61
- Massaro, F., D’Abrusco, R., Tosti, G. et al. 2012 ApJ, 750, 138
- Massaro, F., D’Abrusco, R., Gioletti, M. et al. 2013a ApJS, 207, 4
- Massaro, F., D’Abrusco, R., Paggi, A. et al. 2013b ApJS, 206, 13
- Massaro, F., D’Abrusco, R., Landoni, M. et al. 2015a ApJS, 217, 2
- Massaro, E., Maselli, A., Leto, C. et al. 2015b Ap&SS, 357, 75
- Massaro, F., Landoni, M., D’Abrusco, R. et al. 2015c, A&A, 575, 124
- Massaro, F., Thompson, D. J., Ferrara, E. C. 2016 A&AR, 24, 2
- Massaro, F., Álvarez Crespo, N., D’Abrusco, R. et al. 2016c ApSS 361, 337
- Massaro, F. & D’Abrusco, R. 2016 ApJ, 827, 67
- Massaro, F., Marchesini, E. J., D’Abrusco, R., Masetti, N., Andruchow, I., Smith, H. 2017 ApJ, 834, 113
- Mauch, T., Murphy, T., Buttery, H. J., Curran, J., Hunstead, R. W., Piestrzynski, B., Robertson, J. G., Sadler, E. M. 2003, MNRAS, Volume 342, p. 1117
- Nolan, P. L., Abdo, A. A., Ackermann, M. et al. 2012 ApJS, 199, 31
- Nori, M., Giroletti, M., Massaro, F. et al. 2014 ApJS 212, 3
- Paggi, A., Massaro, F., D’Abrusco, R. et al. 2013 ApJS, 209, 9
- Paggi, A., Milisavljevic, D., Masetti, N. et al. 2014 AJ, 147, 112
- Petrov, L., Mahony, E. K., Edwards, P. G. et al. 2013 MNRAS, 432, 1294
- Ricci F., Massaro F., Landoni M. et al. 2015 AJ, 149, 160
- Saxton, R. D.; Read, A. M.; Esquej, P. 2008, A&A, 480, 611
- Sbarufatti, B.; Treves, A.; Falomo, R.; Heidt, J.; Kotilainen, J.; Scarpa, R. 2006, AJ, 132, 1S
- Schinzel, F. K., Petrov, L., Taylor, G. B. 2015 ApJS, 217, 4
- Schlegel, David J.; Finkbeiner, Douglas P.; Davis, M. 1998 ApJ 500 525S
- Seibert, M, Wyder, T., Neill, J., Madore, B. et al. 2012 American Astronomical Society Meeting Abstracts, 219, 340.01
- Stickel, M., Padovani, P., Urry, C. M. et al. 1991 ApJ, 374, 431
- Skrutskie, M. F., Cutri, R. M., Stiening, R., et al. 2006, AJ, 131, 1163
- Takeuchi, Y., Kataoka, J., Maeda, K. et al. 2013 ApJS, 208, 25
- Taylor, M. B. 2005, ASP Conf. Ser., 347, 29
- Tody, D. 1986, SPIE, 627, 733
- Urry, C. M., & Padovani, P. 1995, PASP, 107, 803
- Voges, W., Aschenbach, B., Boller, T., et al. 1999, A&A, 349, 389
- Voges, W., Aschenbach, B., Boller, T., et al. 2000, IAUC, 7432R, 1
- Warwick, R. S., Saxton, R. D., & Read, A. M. 2012, A&A, 548A, 99
- White, R. L., Becker, R. H. Helfand, D. J., Gregg, M. D. et al. 1997 ApJ, 475, 479
- Wright, A. E., Griffith, M. R., Burke, B. F., & Ekers, R. D. 1994, ApJS, 91, 111
- Wright, E. L., et al. 2010 AJ, 140, 1868